AB INITIO STUDY OF SURFACE ENERGY, SURFACE STRESS AND COUPLING COEFFICIENT OF Au (111)

BY

SHEHU MUSTAPHA

40983

A THESIS PRESENTED TO THE DEPARTMENT OF THEORETICAL AND APPLIED PHYSICS, AFRICAN UNIVERSITY OF SCIENCE AND TECHNOLOGY ABUJA NIGERIA IN PARTIAL FUFILLMENT OF THE REQUIREMENTS FOR THE AWARD OF MASTER OF SCIENCE IN THEORETICAL AND APPLIED PHYSICS

December, 2023

AB INITIO STUDY OF SURFACE ENERGY, SURFACE STRESS AND COUPLING COEFFICIENT OF Au (111)

By

SHEHU MUSTAPHA

40983

A THESIS SUBMITTED TO THE DEPARTMENT OF THEORETICAL AND APPLIED PHYSICS, AFRICAN UNIVERSITY OF SCIENCE AND TECHNOLOGY ABUJA NIGERIA IN PARTIAL FUFILLMENT OF THE REQUIREMENTS FOR THE AWARD OF MASTER OF SCIENCE IN THEORETICAL AND APPLIED PHYSICS

SUPERVISED BY

Dr. Abdulhakeem Bello
Dr. Okikiola Olaniyan

DECEMBER, 2023

DECLARATION

I, SHEHU MUSTAPHA with student identification number **40983** hereby declare that this thesis titled "Ab initio study of surface energy, surface stress and coupling coefficient of Au (111)" was written by me under the supervision of **Dr. Abdulhakeem Bello** and **Dr. Okikiola Olaniyan** in the Department of Theoretical and Applied Physics, African University of Science and Technology [AUST], Abuja - Nigeria. All information derived from various literatures have been dully acknowledge, listed and cited. No part of this work has been presented by any other person(s) for the award of any degree at other institution(s).

THESIS APPROVED BY

A thesis approved by the Department of Theoretical and Applied Physics, African University of Science and Technology [AUST], Abuja - Nigeria.

RECOMMENDED: ……..

Supervisor: Dr. Abdulhakeem Bello

……

Co-Supervisor: Dr. Okikiola Olaniyan

……

Dr. Anatole Kenfack

[Head of Department]

APPROVED: ……

[Chief Academic Officer]

DEDICATION

This thesis is dedicated to Almighty Allah (SWT) our sustenance, my father, my mother and my Siblings.

ACKNOWLEDGEMENT

All praises and adoration are due to Allah the lord of the world who has given me the opportunity in all kinds to acquire this, Degree. May His peace and blessings be upon our noble prophet Muhammad (S.A.W) and his righteous companions. My appreciation goes to my father, Mother, siblings and relatives for their love and support. My sincere appreciation goes to my dynamic and courageous supervisors Dr. Abdulhakeem Bello and Dr. Okikiola Olaniyan for their relentless support throughout the course of this thesis. A big thanks to the Head of the Department of Theoretical and Applied Physics, Dr. Anatole Kenfack and all staff of the Theoretical and Applied Physics Department, African University of Science and Technology for the unquantifiable knowledge they have imparted on me during my period of study.

I would like to acknowledge or providing me access to CHPC Lengau Cluster to performed all the calculations presented in this thesis. I must thank Federal University Dutse for sponsoring my master's studies through the Tertiary Institution Trust Fund (TETFUND). I appreciate the support and guidance of Dr. Usman Bello Abdulmalik of the Department of Pure and Applied Mathematic African University of Science and Technology, Dr. Hafeez Yusuf Hafeez of the Department of Physics Federal University Dutse, Dr Dahiru Muhammad Sanni of the Department of Physics Federal University Dutsin–Ma and my colleagues in the Department of Physics Federal University Dutse.

Special gratitude to my colleagues Tahir Abdullahi, Faruk Baffa Usman, Amina Muhammad Tanimu, Jide Adegboyega, Tolani Oladipo, Kingsley Chibuike, and Gideon Korir for their collaboration, sharing of ideas and friendship during our master's degree program.

TABLE OF CONTENT

CONTENTS **PAGE**

TITLE PAGE……. i

DECLARATION PAGE……. ii

THESIS APPROVED……... iii

DEDICATION…….. iv

ACKNOWLEDGEMENT……. v

TABLE OF CONTENTS…… vi

LIST OF TABLES…… ix

LIST OF FIGURES…… x

ABSTRACT…….. xi

CHAPTER ONE: **INTRODUCTION**……... 1

1.1 Background of the Study…… 1

1.2 Statement of the Problem…….. 4

1.3 Aim of the Study…….. 4

1.4 Objectives of the Study…….. 4

1.5 Justification of the Study…… 5

1.6 Scope of the Study…… 5

CHAPTER TWO: **LITRERATURE REVIEW**……. 6

2. 1 Conceptual Review…….. 6

2.1.1 Gold (Au)…… 6

2.1.2 Surface Energy…… 7

2.1. 3 Surface Stress……. 8

2.1.4 Work Function……. 9

2.1.5 Electrocapillary Coupling Coefficient (ς) …….. 10

2.2 Theoretical Framework…… 11

2.2. 1 First-Principles Calculations……. 11

2.2.2 Density Functional Theory (DFT)……. 12

2.2.3 The Hohenberg - Kohn (HK) Theorems……. 13

2.2.4 The Kohn-Sham (KH) Equations…….. 15

2.2.5 Exchange-correlation functions…… 16

2.2.6 The Local Density Approximation (LDA)…… 17

2.2.7 The Generalized Gradient Approximation (GGA)..... 18

2.2.8 LDA + U…….. 19

2.2.9 Plane Wave Basic Set…….. 21

2.2.10 Pseudopotential……. 21

2.2.10.1 Norm-conserving Pseudopotential……. 22

2.2.10.2 Ultrasofts Pseudopotentials (USPPs)……. 22

2.2.10.3 Projected – Augmented Wave (PAW)…… 23

2.3 Empirical Review…… 23

CHAPTER THREE: **METHODOLOGY**…….. 29

3.1 Introduction…… 29

3.2 Computational Details……. 29

3.2.1 Kinetic energy cut-off (Ecut) Optimization…… 29

3.2.2 The K-point Optimization…… 30

3.2.4 Surface Optimization…….. 31

3.3 Implementation of strain…… 31

3.4 Calculation of the Surface stress…… 32

CHAPTER FOUR: RESULT AND DISCUSSION……. 36

4.1 Results from Parameters Optimization Calculation…… 36

4.2 Result of the Computation of Surface Energy…… 42

4.3 Results from the Computation of Surface Stress…… 44

4.3 Result from the Computation of Coupling Coefficient…….. 47

CHAPTER FIVE: **CONCLUSION AND RECOMMENDATIONS**……. 49

5.1 Conclusion…….. ….. 49

5.2 Recommendations…….. 49

References……. 50

LIST OF TABLES

Table No.	Title	Page
2.1	Work function, surface stresses and coupling coefficient reported by [9]	24
2.2	Surface energies and work functions reported by [7] for some metals.	25
4.1	Total energy convergence with energy cutoff.	36
4.2	Results of Kpoints convergence with total energy	38
4.3	Results of total energy convergence with lattice parameters.	40
4.4	Result for the computation of surface energy.	42
4.5	Results of applied strain and energy for bulk and slab.	44
4.6	Variation of applied strain with work function.	47

LIST OF FIGURES

Figure No.	Title	Page
3.1	Au (100) conventional unit cell	34
3.2	Au (111) bulk and slab super cells	36
4.1	Plot showing the total energy plotted against the energy cut – off	38
4.2	Plot showing the total energy plotted against the energy K - Points	40
4.3	Plot showing the total energy plotted against the lattice parameter	42
4.4	Plot showing the total energy per unit cell against number of layers	44
4.5(a)	Plot showing the total energy against strain applied for bulk deformation along x-axis	46
4.5(b)	Plot showing the total energy against strain applied for slab deformation along x-axis	47
4.6	Plot showing variation of strain applied with work function	49

ABSTRACT

This study investigates ab initio exploration of the Au (111) surface within the generalized gradient approximation, with a primary focus on assessing the convergence properties of this noble metal. An in-depth analysis of the material's response to various computational parameters, including cutoff energy, K-point sampling, and lattice parameter, was conducted to ensure the reliability and consistency of the findings. The theoretical determination of the lattice constant, yielding a value of 4.059 Å, not only aligns quantitatively with experimental measurements but also agrees with calculated values. A noteworthy aspect of this investigation involves reporting on the work function's response to strain, shedding light on how this essential property evolves under external influences. Additionally, the study evaluates the variation of energy per unit cell with varying slab thickness, providing insights into the material's behavior across different structural configurations. The results reveal that Au (111) exhibits a surface energy of 0.5561 $eV\text{Å}^{-1}$, surface stress of 0.18177 $eV\text{Å}^{-2}$and a coupling coefficient of 1.145 eV. These results provides significant implications for understanding the mechanisms associated with electrochemical coupling at an atomic scale, offering crucial insights into the material's behavior across diverse atomic and electronic structures. Thus this work contribute to the understanding of Au (111) surface properties, laying a foundation for advancements in understanding electrochemical phenomena and fostering the development of tailored applications in materials science and nanotechnology.

CHAPTER ONE

INTRODUCTION

1.1 Background of the Study

A crystal's surface serves as the primary interface between a solid material and its surroundings, consequently the study of surfaces has implications indubitable for catalytic activity and growth rate of a solid's [1,2]. The surface of a solid material is the site of several important chemical reactions, including catalysis and adsorption. Consequently, accurately determining a solid surface's energy provides important insight into the material's potential applicability in these processes [1]. Typically, when modeling a solid surface, an extremely periodic representable of the atomic configuration of the interior of a crystal (bulk material) is cut from a representable of the atomic configuration of a crystalline surface (slab model). Two surfaces of the slab, the topmost and bottommost, were concurrently stripped by a slab cleave, each with a comparable Miller index. Some materials cleft to produce symmetric slab models with similar upper and lower surface edges, while other materials cleave to produce precisely matched structural and stoichiometric slab models with two different surface edges with different atomic positions and properties (asymmetric slabs) [1]. The surface layer of a crystal might decrease its energy by optimization of the atomic layers in a path perpendicular to the surface or by surface rebuilding in which the periodicity of the rebuilt layer is unlike that of the bulk. The smallest energy configuration of the crystal will have the surface layer stressed in its particular plane, whereas the bulk material resist the stress so that equilibrium is attained. i. e. the total stress due to both surface and bulk material is zero[3]. The investigation of the surface geometry of solid surfaces is one of the fundamental subjects of surface science. Metals (such as gold) surfaces are of particular concern, because they

act as catalysts in several hydrogenation and reduction processes. It is well known that actual surfaces of clean metals can implement structures changes from those of preferably truncated crystals[4]. The energy of a surface is an imperative physical variable in monitoring extensive series of phenomena like the stress for brittle fracture, the growth rate during particle coarsening and the rate of sintering and [5].

In a metal nanocrystals the surface energies determine equilibrium form which account for the relative stability of several crystallographic planes[6]. Surface energy and work function are essential physical variables of metallic surface, they are vital to appreciate an extensive variety of surface phenomena[4, 5]. These phenomena comprise surface segregation, adsorption, surface corrosion, catalytic behavior, growth rate, and the formation of grain boundaries[1, 4]. The equilibrium shape of crystals is determining surface energy and work function. Different crystal alignments and the surfaces relaxation have an effect on the amount of the surface energy and work function[7]. The surface energy and work function calculated with hypothetical approaches particularly by the density functional theory are showed to be an effective way to obtain the reasonable outcomes. A lot of researches have been done in this field. Kokko et al.

Current researches shows a macroscopical expansion or contraction when high surface area metals with nanometer-sized absorbency are electrically exciting, the sign of changes in the surface bond forces once a space-charge layer is produced[9]. The variable which computes these forces in the continuum explanation of solid surfaces, the surface stress, f, is a matter of attention recently in surface science, subsequently it is complicatedly connected to the surface electronic structure and bonding, and meanwhile it is applicable for modernization as well as for the stress in thin film devices[7,8]. Computations of electronic-structure are attractive and broadly applied to increasingly intricate and practical materials systems and devices, delving deeply into the field of

nanotechnology with uses that include semiconductors and metal molecule junctions, field effect transistors made of carbon nanotubes, and nanostructured metals. It is vital and critical to have a strong background or knowledge of the fundamental concepts of the metal main surfaces preliminary surface energies, structural relaxations, and work functions[8].

Electrocapillary coupling variable close to the charge-neutral surface (potential of zero charge) could be determined in terms of the response of the electronic work function to an applied in-plane strain[9, 11]. The surface stress's response to a change in the superficial charge density is known as the coupling parameter [12]. For nominally clean surfaces, it fundamentally describes a conversion of electrical energy to mechanical work or vice versa and therefore is sometimes also referred o as electromechanical coupling parameter. Meanwhile and the work function of the metal surface and the electrode potential are closely related. Hence, first-principles values for the coupling coefficients between work function and strain will be accompanied by an analysis of the response [11]. The term electrocapillary coupling and are related to the modification of the surface stress, a capillary parameter of solid surfaces, due to changes of state of the surface [13]. While experimentally these phenomena are typically observed at the solid-electrolyte interface. the surface stress has to be balanced by corresponding stresses in the bulk, materials with a high surface-to-volume ratio react with a detectable deformation to changes in their surface stress [14, 15]. Experiments testify to a variation of the coupling coefficient with the electrode potential that is dependent on which processes are active at the electrode surface[14-16]. A precise instance for the implication of the electrocapillary coupling strength is the catalytic activity of compositionally categorized surfaces, for example in core–shell catalyst particles [16].

1.2 Statement of the Problem

The deficiency of an ordinary technique strictly hinders the computational determination of the low-energy surfaces of materials that cleave irregularly. However density functional electronic structure calculations are used usually to examine materials, researches reporting surface energies for asymmetric slabs calculated using first principle approaches remain insufficient, specifically studies of the exactness and convergency of the computations [1]. Experiment find it problematic with several faults to determine the absolute value of the surface energy of a solid directly[1,11]though the surface energy (or surface tension) in the liquid state has been measured for most metals precisely more than solid [5,10], so ab initio theoretical calculations are a valuable alternative approach[1, 9].Typical density functional theory means depend on the local or semi-local calculation to the many-body functional relating exchange-correlation. Even though many dependable estimates were perform by DFT regarding structural and thermodynamical stabilities there are great classes of materials, for which the normal DFT applications be unsuccessful and are not predictive [19].

1.3 Aim of the Study

The aim of this research is to study the coupling coefficient of Au (111) surface through comprehensive ab initio computational methods.

1.4 Objectives of the Study

The study has the following objectives.

i. To optimize the lattice parameters, different energy cutoff values and K-Points mesh in the Brillouin zone to ensure reliable and efficient accuracy and convergence of the computational outcomes.

ii. To analyze the surface optimization of the Au (111) slab.

iii. To correlate the results obtained from the various computational studies to draw comprehensive conclusions about the coupling coefficient of Au (111).

1.5 Justification of the study

The findings of this research will add to the existing literatures in the topic and provide room for further research in the related topics. The outcomes of this work will be useful in comparison with the experimental and other theoretical values.

1.6 Scope of the Study

The research is geared towards studying the coupling coefficient of Au (111) plane using density functional theory method. Convergence tests of the energy cut off, K-Points, and lattice constant will be carried out. VASP software installed on high performance computer (HPC) will be use to run all the calculations. The variability of the parameters computed will be represented graphically which will provide information about the Au (111) plane surface.

CHAPTER TWO

LITERATURE REVIEW

2.1 Conceptual Review

In order to understand surface behaviors such as surface energy, stress, work function it is important to discuss some terms associated to crystals surface among other things.

2.1.1 Gold (Au)

Gold is an expensive metal with a distinctive cheerful and attractive type recognized as the golden yellow color. As of 2012, a overall of 174,100 tons of Au has been extracted in olden times of human, which, in terms of volume, corresponds to roughly 9020 m^3, or simply a solid cube of 21 m on each side [20, 21]. For long gold been observed as an "inert" surface and it bulk surface cannot chemisorb several molecules without difficulty [20, 21]. Nevertheless, in the previous decade, mainly through the efforts of [21, 22], the particles of gold, predominantly those less than 5 nm in size, have received exclusive consideration for catalytic properties, jewellery, and as coinage metal [20, 23]. Unadulterated elemental gold has an exceptional color and shine which has captivated human beings for years [26], in the hydrochlorination of acetylene a gold-based catalyst can be used [27]. Gold has admirable conductivity as a conductor for electrical applications [26]. The malleable and ductile properties of gold make it compressible or stretchable to subjective shape [28]. Gold can be relatively biocompatible, as some edible gold foils are added to cakes, tea, and cosmetics [29]. Functionalization of gold nanoparticles is crucial for the effective utilization of these materials in health related application s[26]. At small temperatures, when gold is slightly sufficient—with particle diameters below 10 nm—it turns out to be amazingly vigorous for numerous reactions, such as propylene, epoxidation and CO oxidation [30, 23, 24].

2.1.2 Surface Energy

Surface energy is the amount of energy required to create a new surface (is the energy required to split an infinite crystal into two fragments) [7, 8]. Determining this quantity experimentally is challenging because it usually necessitates measuring surface tension at the melting point of metals [5,8]. Its value is necessarily positive, otherwise bulk matter would be unstable with respect to fragmentation [11]. In materials modelling, Surface energies can be obtained from first-principles calculations in two ways [31], one may use slabs of different thicknesses and extract from them the energy of a bulk atom. Alternatively, Finding the energy of a surface termination involves dividing the total energy of a slab model with relaxed atoms (E_{slab}) by the total energy of an equivalent quantity of relaxed bulk material (NE_{Bulk}), and then dividing the result by the total area exposed in the slab model, which is twice the area of a single face [8,36], according to the following expression[1, 8, 36];

$$\sigma = \lim_{N \to \infty} \frac{1}{2}(E_{Slab}^{N} - NE_{bulk}) \qquad (2.1)$$

Where, E_{Slab}^{N} and NE_{bulk} are the total energies an N-atom slab and the bulk per atom respectively. The two surfaces in the slab unit cell are taken into account by the factor ½. However, if there are numerical changes between the calculation for the bulk and the slab, such as adjustments to the k-point mesh, etc., equation (2.1) will diverge with increasing slab thickness [1, 8, 36].

In order to avoid this nonconvergence two approaches have been proposed by [36] and [37] to determine surface energies. the bulk energy in equation (2.1) was used by [32] as $E_{Slab}^{N} - E_{Slab}^{N-1}$, hence sidestepping a calculation on a distinct bulk system and efficiently removing the errors from differences in K-point sampling. [33], modified equation (2.1) by considering the limit of large N as follows;

$$E_{slab}^{N} = \approx 2\sigma + NE_{bulk} \qquad (2.2)$$

By avoiding a calculation on a separate bulk system, the bulk energy term E_{bulk} can be considered as the slope and used in equation (2.1) if the total energy of the slab depends linearly on the thickness N of the slab. When large and matching K-point samplings are used, it has been found that divergence can be avoided in practice for both slab and bulk calculations [31].

2.1. 3 Surface Stress

One of a material's most important and fundamental mechanical properties, strength quantifies the material's capacity to support a load. A material's yield, or fracture, causes a decrease in its load-bearing capacity or, in extreme situations, its loss of functionality [34]. It is necessary to balance the surface stress, f, at a solid's surface by offsetting bulk stresses. The resulting surface-induced bulk stresses in materials with a nanoscale microstructure can be significant and have a significant impact on the material's behavior. Considerable changes to the magnetic and alloy phase diagrams are among the effects [16, 39]. The reversible work per unit area needed to stretch the surface elastically is known as the surface stress. Accordingly, it is equivalent to the derivative of the surface energy in relation to the in-plane strain [11].

The surface induced stress can have shear components which, at very small size, result in a shear instability of the crystal lattice. This imposes lower limits on the size of stable nanoscale objects or microstructures[16, 40]. Since the strain state of a two-dimensional surface is represented by a second rank tensor[11], the surface stress is also a second rank tensor, whose components are given by

$$f_{ij} = \frac{d\gamma}{d\varepsilon_{ij}} \tag{2.3}$$

with $\varepsilon_{i\,j}$ being the components of the surface strain tensor. The interface stress was primarily indicated by the parameter, f. If f and e are represented as 2 x 2 tensors in the tangent plane, and strain and area are measured in relation to a reference state in the solid, then f is symmetric [34].

2.1.4 Work Function

The work function which measure the behavior of electrons in a material, is regarded as a key term in surface science to recognize the corrosion rates and interfacial engineering in the manufacture of photosensitive and electron-emitting devices [36]. It is a fundamental surface electronic property of a material [37]. Materials with a low work function emit electrons easily into space and form an important factor for electronic devices used widely in applications from satellite communications to thermionic energy conversion [38]. Work function is the is the lowest amount of energy required to eject [7, 41] an electron from the surface of a material [39]. Different authors [45, 46, 47] asserted its dependence on physical factors such as temperature, surface dipole, doping, and electric field. The contribution of image potential to the work function of materials, which is temperature-dependent, is a significant finding that has been extensively studied by researchers [41, 48, 49]. Theoretical and experimental results displayed that work function is dependent on thermal expansion of the lattice, Young's modulus, heat capacity [45], corrosion, friction, surface energy, adhesion fracture toughness, , and yield strength and hardness [51, 52, 41].

In terms of the density functional theory, the work function can be evaluated as the difference between the electrostatic potential value in the vacuum region (i. e. vacuum level) and the Fermi energy [47] given by

$$W = V_{dip} - E_f \tag{2.4}$$

With $V_{dip} = V_{vacuum} - \hat{V}_{bulk}$ as the energy needed to stab the dipole barrier that is formed by the redistribution of electronic charge at the surface and the Fermi energy E_f is the energy of the maximum occupied state in the bulk metal. Experimentally, the work function may be determined e.g. by photoelectron spectroscopy or the Kelvin probe technique, where the latter is restricted to relative measurements But the results are often inaccurate due to the drawbacks of SKPFM itself [7]. The work function is also sensitive to the condition of the surface, e.g. it is affected by adsorption of contaminants. Adsorption of atomic or molecular species may change the work function due to (i) charge transfer between adsorbate and surface, (ii) polarization of substrate and adsorbate charge densities and (iii) their permanent molecular dipole moment. [11]

2.1.5 Electrocapillary Coupling Coefficient (ς)

Electrochemical investigations can deliver mostly comprehensive and detailed evidence on the surface stress variation during changes of state at the solid surface [16]. A key parameter in such experiments is the electrocapillary coupling coefficient [16].The electrocapillary coupling coefficient, ς, determines the response of the electrode potential, E, to tangential elastic strain at the surface of an electrode by means of dynamic electro-chemo-mechanical analysis [18].

The phenomenological context of electrocapillary coupling is depend on a surface free energy density (per area) Ψ, which describes the properties of the interface between metal electrode and electrolyte that differ from those of the adjacent bulk phases [11]. The state variables of Ψ are the tangential strain, e relative change in surface area, A and the superficial charge density $q = \frac{Q}{A}$, where Q is the total charge at the surface. As the second derivative of the state function Ψ the variation of the surface stress with the superficial charge density is a fundamental materials variables, the so-called electrocapillary coupling coefficient [11, 16] is given by

$$\varsigma = \frac{df}{dq} \tag{2.5}$$

The coupling coefficient, varies with the electrode potential, and is distinctive for the acting electrode process [16]. Meanwhile the surface stress is coupled to the bulk stress state through balance laws, materials with a high surface-to-volume ratio respond with a measurable elastic deformation to surface stress variation [11]. A precise instance for the implication of the electrocapillary coupling strength is the catalytic action of compositionally grouped surfaces, for instance in core–shell catalyst particles, electronic structure, relaxation and for the charge transfer between electrode and adsorbate [16, 53]. Moreover, ς provides the efficiency of surfaces in permitting nano porous metal propulsion and current experimentations reveal its vital role in computing the coupling between mechanics and reactivity in strained-layer catalysts [18].

2.2 Theoretical Framework

2.2. 1 First-Principles Calculations

The first principles approaches are developed based on the density functional theory (DFT) by Kohn *et al*. The main advantage of this approach is change from a wave function, depending on the coordinates of all electrons, to a charge density depending on the three three-dimensional coordinates only [49]. The first principles method or *Ab initio* is a method that necessitates only the basic properties such as atomic number, atomic radius, nuclear-charge density, and others as inputs. These primary inputs together with vital scientific rules can produce the true state of a physical system without the assistance of any empirically adjustable parameter.

The first-principles procedures consider nuclei and electrons as the basic particles and describe events in a sub - atomic world. Consequently, the system can be expressed only by quantum mechanics that contains relatively problematic partial differential equations. Consequently, first-

principles calculations are independent of any external parameters excluding the atomic numbers of the constituent atoms to be simulated [50]. In this work first – principles technique will be employed for obtaining all the results.

2.2.2 Density Functional Theory (DFT)

In physics, materials science, chemistry, and many engineering fields, the use of density functional theory (DFT) computations is quickly becoming a common tool for a variety of materials modeling problems [57]. Density functional theory is the model, in which properties of many-body systems can be computed using functions of another functions (i.e. functionals) depending on electron density. Density functional theory (DFT) is a low-cost, time-saving quantum mechanical model, used to calculate several physical characteristics of solids with high precision [53]. DFT belongs to the family of first principle or ab initio methods because they can predict materials properties for an unidentified system without any experimental input.

In 1926 with the formation of Thomas- Fermi theory, an approximate method for finding the electronic structure of atoms by means of just single electron ground-state density, ρ (r), but too crude to bind molecules. In the 50's, Slater intuitively joined this idea with Hartree's orbital method in the X_α scheme. Later, the Hohenberg-Kohn (HK) theorem showed that a precise method based on ρ (r) exists in principle. The modern type in use today is Kohn- Sham (KS) DFT, which explains a self-consistent equation that must be solved for a set of orbitals whose density, ρ(r) is defined to be exactly that of the real system [54]. The DFT has its initiation from Hohenberg-Kohn theorem whose stated outwardly two simple theorems in 1964 that facilitated the execution of DFT [54].

2.2.3 The Hohenberg - Kohn (HK) Theorems

The DFT has its initiation from Hohenberg-Kohn theorem whose stated outwardly two simple theorems in 1964 that facilitated the execution of DFT [55]. The first theorem state that the external potential, $V_{ext}(\vec{r})$ is a unique functional of electron density $\rho(\vec{r})$, with a unique link between potential and electron density for a many body system; $V_{ext}(\vec{r}) \implies \rho(\vec{r})$, although this electron density can be used to describe the whole information of the system [54]. In order to form a mathematical relation, let us assume external potentials as $V(r)$ and $V(r')$ while the change among these potentials is constantly identical subsequently the ground state electron density is similar at whole parts of the crystal, that is, $V(r) - V(r')$ = constant. According to theory, electrons travel in a field created by external potential V_{ext} and interact with one-another in addition to their external potential, and the corresponding Hamiltonian of energy [60] can be written as

$$H = T + V_{ext} + U \tag{2.6}$$

Where T, V_{ext} and U, represents the kinetic energy (K.E) of electrons, external potential and coulomb interaction respectively. Quantum mechanically the factors T, U, and V_{ext} can be expressed as[55]

$$T = \frac{1}{2} \int [\nabla\psi^*(r)\nabla\psi(r)]\, dr \tag{2.7}$$

$$V = \frac{1}{2} \int [\mathrm{v}(r)\psi^*(r)\psi(r)]\, dr \tag{2.8}$$

$$U = \frac{1}{2} \int \left[\psi^*(r')\psi^*(r)\psi(r')\psi(r)\frac{1}{|r - r'|}\right] drd \tag{2.9}$$

The solution of Hamiltonian for Equation. (2.6) can be expressed as;

$$H\psi(r_1, r_2, \ldots\ldots\ldots, r_N) = E\psi(r_1, r_2, \ldots\ldots\ldots, r_N) \tag{2.10a}$$

The term $\psi(r_1, r_2, \ldots\ldots\ldots\ldots, r_N)$ is a ground state N interacting particle's wave-function. Suppose an additional potential v'(r) with changed Hamiltonian H' and wave - function Ψ'(r) where the ground state density ρ(r) must remain the same for both cases. The Hamiltonian for this many-body system [55]can be written as

$$H'\psi' = E'\psi' \qquad (2.10b)$$

Following a thorough exploration of the situation, established on v(r) – v(r') is constant, it can be concluded, that ψ(r) and ψ'(r) are different; as a result, they both satisfy distinct Schrodinger wave equations. Similarly, if T and U are known for N-partials systems so ρ (r) may be considered to find ground state H and E. The functional association of minimum energy state and corresponding resulting density is [55]

$$E[\rho(r)] = T[\rho(r) + V\rho(r) + U\rho(r)] \qquad (2.11)$$

The second theorem state that the true ground state density of an electron relates to electron density that minimizes the total energy of the functional. Assume, ρ(r) is the density which is related to ground state while ρ′(r) to any other state of a many-body system. The functional for total energy in this regard is given as; $E[\rho'] > E[\rho]$ Furthermore, suppose that F[ρ(r)] is a general functional that is valid for fixed electrons at all external potentials, this can be express [55] Mathematically as

$$F[\rho(r)] = T[\rho(r)] + U[\rho(r)] \qquad (2.12)$$

Similarly,

$$E[\rho(r)] = \int [\mathrm{v}(r)\rho(r)dr] + F[\rho(r)] \qquad (2.13)$$

In order to have minimum energy functional, the consistent density ρ(r) must be principally a ground state density [55];

$$E[\psi'] = V\psi', + (\psi', \ T + U)\psi' \qquad (2.14)$$

2.2.4 The Kohn-Sham (KH) Equations

The theorems specified by Hohenberg-Kohn are precise; nevertheless, not very applicable in actual computations [60, 61]. In order to approximate the kinetic and electron-electron functionals, Kohn and Sham [57] proposed the following method: they introduced a hypothetical system of N non-interacting electrons that would be described by a single determinant wave function in N "orbitals ϕ_i" *fi*. The orbitals in this system provide precise information about the kinetic energy and electron density [57].;

$$T_s[\rho] = \frac{1}{2}\sum_{i}^{n}\langle\phi_i|\nabla^2|\phi_i\rangle \qquad (2.15)$$

The suffix now emphasizes that this is the kinetic energy of a system of non-interacting electrons, which replicates the actual ground state density, rather than the true kinetic energy. [55, 57];

$$\rho(r) = \sum_{i}^{n}[\phi_i]^2 \qquad (2.16)$$

Since the density can be constructed from an asymmetric wave function, it is guaranteed to be legal when it is constructed explicitly from a set of orbitals. If we further observe that the classical Coulomb interaction, or Hartree energy (which is just the terms of Equation (2.9) expressed in terms of density, will constitute a substantial portion of the electron-electron interaction;

$$\mathrm{V_H}\,[\rho] = \frac{1}{2}\int\frac{\rho(r_1)\rho(r_2)}{|r_1 - r_2|}dr_1 dr_2 \qquad (2.17)$$

As a result, the energy functional is rearranged as follows:

$$\mathrm{E}[\rho] = T_s[\rho] + V_{ext}[\rho] + V_H[\rho] + E_{xc}[\rho] \qquad (2.18)$$

Where $\mathrm{E_{xc}}$ is the exchange-correlation functional [55], [57] given as ;

$$E_{xc}[\rho] = (T[\rho] - T_s[\rho]) + (V_{ext}[\rho] - V_H[\rho])$$

E_{xc} is the total of the errors made when applying a kinetic energy that is not interacting and when taking the electron-electron interaction into account in a classical manner. The following set of equations is satisfied by the orbitals that minimize the energy, according to the variational theorem;

$$\left[-\frac{1}{2}\nabla^2 + V_{ext}(r) + \int \frac{\rho(r')}{[r - r']} dr' + V_{xc}(r)\right]\phi_i(r) = \varepsilon_i \phi_i(r) \qquad (2.19)$$

in which the functional derivative of the exchange correlation energy with respect to density is introduced as a local multiplicative potential (Kohn and Sham, 1956);

$$V_{xc}(r) = \frac{\delta E_{xc}[\rho]}{\delta \rho} \qquad (2.20)$$

The behaviour of non-interacting "electrons" in an effective local potential is described by this set of non-linear equations, also known as the Kohn-Sham equations. Equations (2.16) and (2.18), respectively, yield the exact ground state density and ground state energy for the exact functional, and hence exact local potential, derived from the "orbitals". With the local exchange-correlation potential V_{xc} in place of the non-local exchange potential, the Kohn-Sham equations share the same structure as the Hartree-Fock equations. E_{xc} is not the sum of the correlation and exchange energies as stated in the correlated wave function and Hartree-Fock theories; rather, it includes a component of the kinetic energy. The density and ground state energy of a system containing non-interacting Fermions and the "real" many systems described by the Schrödinger equation [57].

2.2.5 Exchange-correlation functions

The exchange-correlation energy functional's form is necessary for the Kohn-Sham equations to be used practically, but the precise form of E_{xc} is unknown and might never be known (in a closed mathematical form). Consequently, since the development of DFT, approximations for Exc have

been used in various ways (Santra, 2010). The final term is XC energy, which is composed of all quantum effects and is approximated in terms of electron density [50]

$$E_{XC} = E_X + E_C \tag{2.21}$$

The correlation energy between electrons with a different spin is called Ec, and the exchange energy between electrons with the same spin is called Ex.

2.2.6 The Local Density Approximation (LDA)

The local density approximation (LDA), which rose to popularity in solids calculations in the 1970s and 1980s [54], is the common exchange correlation approximation. It divides the system's entire inhomogeneous electron region into several small regions and approximates each of these regions as a homogeneous electron gas [58]. The exchange-correlation energy density, $\varepsilon_{Xc}((\mathcal{r}))$, in this model, is taken to be the same at every point, just like in a homogeneous electron gas. The exchange-correlation energy in a spin-unpolarized system takes the following form:

$$E_{XC}^{LDA}[\rho] = \int \rho(\mathcal{r})\, \varepsilon_{Xc}\big(\rho(\mathcal{r})\big) d\mathcal{r} \tag{2.22}$$

The quantity $\varepsilon_{Xc}((\mathcal{r}))$, can be further divided into contributions from correlation and exchange.

$$\varepsilon_{Xc}\big(\rho(\mathcal{r})\big) = \varepsilon_X\big(\rho(\mathcal{r})\big) + \varepsilon_c\big(\rho(\mathcal{r})\big) \tag{2.23}$$

Bloch and Dirac derived $\varepsilon_X\big(\rho(\mathcal{r})\big)$ as the exchange component of the uniform electron gas.

$$\varepsilon_X = -\frac{3}{4}\left(\frac{3\rho(\mathcal{r})}{\pi}\right)^{\frac{1}{3}} \tag{2.24}$$

The total exchange-correlation energy for the spin-polarized system is expressed as

:

$$E_{XC}{}^{LDA}[\rho_\uparrow, \rho_\downarrow] = \int \rho_\uparrow(\boldsymbol{r})\varepsilon_{XC}\big(\rho_\uparrow(\boldsymbol{r})\big) + \rho_\downarrow(\boldsymbol{r})\varepsilon_{XC}\big(\rho_\downarrow(\boldsymbol{r})\big) d\boldsymbol{r}. \tag{2.25}$$

The spin-unpolarized functionals are used to describe the exchange component.

$$[\rho\uparrow, \rho\downarrow] = \frac{1}{2}((2\rho\uparrow) + (2\rho\downarrow)) \quad (2.26)$$

Where $\rho\uparrow$ and $\rho\downarrow$ respectively, represents the spin-down and spin-up densities. Both the relative spin-polarization and the electronic density determine the spin-dependent correlation energy.

$$\zeta = \frac{\rho\uparrow - \rho\downarrow}{\rho\uparrow + \rho\downarrow} \quad (2.27)$$

The correlation energy E_C [ρ, ζ] is made to interpolate extreme values ζ=0, ±1. If the non-homogeneity of electronic density is ignored, the LDA scheme leads to numerous errors, including incorrectly estimating the binding energy, underestimating the atomic ground-state energy, and mispredicting the semiconductors' energy gap [58]. $\nabla\rho$(r)

2.2.7 The Generalized Gradient Approximation (GGA)

In order to account for the non-homogeneous electron gas in a real solid, such as ground state energies and molecule and solid geometries, GGAs were developed in relation to LDAs by including the gradient of the charge density, $\nabla\rho$(r). This allowed GGAs to produce more accurate results than LDAs [52]. The Perdew, Burke, and Enerhof (PBE) form of GGAs is the most widely used and prevalent. It was utilized in the computation of amorphous carbon models system, and the exchange-correlation energy [50] can be expressed as follows:

$$E_{XC}^{GGA}[\rho\uparrow, \rho\downarrow] = \int f(\rho\uparrow, \rho\downarrow, \nabla_{\rho\uparrow}, \nabla_{\rho\downarrow})\, d\vec{r}. \quad (2.22)$$

The explicit form for correlation energy is

$$E_C^{GGA}[\rho\uparrow, \rho\downarrow] = \int \rho[(r_s, \zeta) + H(\vec{r}_s, , t)]d\vec{r} \quad (2.28)$$

Where $\vec{r_s}$ is the local Seitz radius ρ given by $\rho = \frac{3}{4\pi r_s^2} = \frac{K_F^2}{3\pi^2}$ and t=|∇n|2φksn dimensionless density gradient.

Three requirements were placed on the function H: it has to approach $-\varepsilon Cunif$ in the rapidly varying limit, be given by its second-order gradient expansion in the gradually varying limit, and have a uniform correlation energy under scaling to the high-density limit. Consequently, the H function formula can be expressed as follows:

$$H = \left(\frac{e^2}{a_0}\right)\gamma\varphi^3\, In\left[1 + \frac{\beta}{\gamma}\, t^2\, \left(\frac{1 + At^2}{1 + At^2 + A^2t^4}\right)\right] \tag{2.29}$$

Where $A = \frac{\beta}{\gamma}\left\langle exp\left|\frac{\frac{-\varepsilon_C^{unif}}{\gamma\varphi^3 e^2}}{a_0}\right| - 1\right\rangle^{-1}$

The exchange energy in GGA is expressed as [59].

$$E_X^{GCA}[n] = \int n(r)\varepsilon_X^{unif}\big(n(r)\big)\, F_X^{GCA}(s)dr \tag{2.30}$$

The exchange enhancement factor, $F_X^{GCA}(s)$ indicates the amount that the exchange energy is enhanced over its LDA value for a given n(r). One GGA differs from another based on the F_x selection. $F_X^{GCA}(s)$ exists in two forms: They are Perdew-Burke-Ernzerhof (PBE) and Becke88 (B88) functionals, which have several different forms;

$$F_X^{PBE}(s) = 1 + \varkappa - \frac{\varkappa}{\left(1+\frac{\mu s^2}{\varkappa}\right)} \tag{2.31}$$

$$F_X^{B88}(s) = 1 + \frac{\beta x(S)^2}{C[1+6\beta x(S) Sinh^{-1}(x)(S)]} \tag{2.32}$$

Whereas C and β in B88 are parameters derived from empirical fitting (empirical), κ and μ in PBE are parameters derived from physical constraints (non-empirical), with κ = 0.804. We return to the LDA exchange when the density gradient is zero, which is represented by the formula $F_X^{GCA}(s) = 1$.

2.2.8 LDA + U

Many approaches were developed to describe strongly correlated systems containing transition metal or rare-earth metal ions with partially filled d or f shells after the failure of the orbital-independent potentials-based local density approximation (LDA) and generalized gradient approximation (GGA) methods. In order to account for the strong electron-electron correlations between the d and f electrons, a number of methods were proposed, including the Hatree-Fock method, GW approximation, the self-interaction correction (SIC) method, and LDA+U. According to Ayuk (2019), the LDA+U method yields the following total energy:

$$E_{DFT+U} = E_{DFT} + E_U = E_{DFT} + E_{Hub} - E_{dc} \quad (2.33)$$

where the double-counting energy of the same electronic interactions is denoted by E_{dc} and the corrective Hubbard functional is represented by E_{Hub}. The entire corrective energy can be expressed in simplified form as

$$E_U = E_{HUB} - E_{dc} = \sum_{I,\sigma} \frac{U^I}{2} Tr[n^{I\sigma}(1 - n^{I\sigma})] \quad (2.34)$$

where $n^{I\sigma}$ is the occupation matrix, and the actual electronic interaction that occurs on-site determines U.

2.2.9 Plane Wave Basic Set

The basic set of a plane wave for a state of vector K is defined according to the equation

$$\langle r|\mathrm{K}+\mathrm{G}\rangle = \frac{1}{\sqrt{N\Omega}} e^{i(\mathrm{K}+\mathrm{G})\cdot r}, \frac{\hbar}{2m}|\mathrm{K}+\mathrm{G}|^2 \leq E_{cut} \qquad (2.35)$$

where NΩ is the crystal volume, Ω is the unit cell volume, and E_{cut} is the plane wave kinetic energy cutoff. The PW basis set for a finite number of plane waves is complete for E$cut \longrightarrow \infty$ and orthogonal

$$\langle \mathrm{K}+\mathrm{G}|\mathrm{K}+G'\rangle = \delta_{\mathrm{G}G'}$$

The component of the plane wave basis can be express in the terms of Fourier transform as

$$|\psi_i\rangle = \sum_G C_{i,\ k+G}\,|\mathrm{K}+\mathrm{G}\rangle \qquad (2.36a)$$

$$C_{i,\ k+G} = \langle K+G|\psi_i\rangle = \frac{1}{\sqrt{N\Omega}}\int \psi_i(r) e^{-i(\mathrm{K}+\mathrm{G})\cdot r}\,dr = \widetilde{\psi_i}(\mathrm{K}+\mathrm{G})\cdot| \qquad (2.36b)$$

PWs are therefore not used as a basis set for electronic structure computation as a substitute for straightforward Fourier analysis: Fourier components up to q~2π/δ on the length scale δ. In a solid, this means $\backsim 4\pi\left(\frac{2\pi}{\frac{\delta}{3\Omega B_z}}\right)^3$ PWs (volume of the sphere of radius q divided by $\Omega B_z = \frac{8\pi^2}{\Omega}$, volume of the Brillouin Zone). Getting rid of core states is necessary because this is not a practical solution. eliminate the wiggles of orthogonality near the nucleus. Pseudopotential (PP) becomes highly significant in reaching the above.

2.2.10 Pseudopotential

The characteristics of the real potential are acted upon by the pseudopotential approach. The important points are to pseudize the remaining valence wave functions, to effectively freeze the nucleus and the core electrons together, and to separate the electrons into two groups according to

their contributing implications. As a result, the number of electrons in a system that must be calculated is significantly reduced, and the valence wave functions are much easier to describe and compute [50]. Normconserving PPs, ultrasoft PPs (USPPs), and projector-augmented wave are the three primary categories of PPs [55].

2.2.10.1 Norm-conserving Pseudopotential

for a norm – conserving pseudopotential the pseudo- and all-electron (AE) charge densities inside the core are constructed to be equal [55, 65]. Both generating and using it positively (+) are easy. Usually, and mostly exclusively, theory and methodological improvements are used for norm-conserving partial differential equations (PPs). Its negative (-) values are quite difficult because a significant loss of transferability results from core radii r_c exceeding the outermost maximum of the valence atomic orbitals. This restriction could result in extremely high plane-wave cutoffs (70 Ry and up) for certain atoms, including 2p elements C, N, O, F, 3d transition metals, and 4f rare earth. Though all-electron orbitals can be "reconstructed" using the PAW transformation, please do not divulge any sensitive information regarding the orbitals near the nucleus. According to Ayuk (2019), this is typically the initial decision and point of origin. To fulfill this requirement, a large number of pseudopotentials are created [50]:

$$\int_0^{r_c} \left|\psi_{pp}(r)\right|^2 dr = \int_0^{r_c} |\psi_{AE}(r)|^2 \, dr \qquad (2.37)$$

With this method, the valence electrons perceive nothing differently because the net charge from the core doesn't change. However, in contrast to AE methods, these PPs only provide the valence charge densities—not the total charge densities [50].

2.2.10.2 Ultrasofts Pseudopotentials (USPPs)

We can actually make the pseudo wave function as flat as an upside-down bowl if we ignore the norm-conserving condition and move the peak position of a wave function further to a greater r_c with reduced peak height in addition to removing radial nodes. Van der Bilt refers to the potentials generated as ultrasoft pseudopotentials. A smaller cutoff energy and fewer pseudo wave functions (PWs) can be used to extend this kind of reduced amplitude pseudo wave function, which can result in up to a tenfold speed increase in computation. Furthermore, USPPs provide solely valence charge densities rather than total charge densities [52]. In all cases where norm-conserving PPs are too hard, ultra-soft PPs are usually employed.

2.2.10.3 Projected – Augmented Wave (PAW)

The frozen core all-electron potential (PAW) can be used to describe projector-augmented wave potentials. The efficiency of the PP and the accuracy of the AE potential are the two goals of this type, which was first presented by Blöchl (1994) and accepted by Kresse and Joubert (1999). Lee (2017) notes that the mapping provides two distinct descriptions for the core and parts of the valence wave functions. The most practical method is projector-augmented wave, which is applicable to even "difficult" atoms for Ultrasoft PPs (such as magnetic materials), and whose accuracy is comparable to that of all-electron techniques, according to the formalism adds more terms and provides information about the orbital close to the nucleus. It is also more difficult to obtain than Ultrasoft PPs.

2.3 Empirical Review

A lot of studies has been carried out to investigate the behavior of a material surface using different experimental and computational techniques. [37] reported the electronic work function of the cu (100) surface under different strain states, these authors find that the tensile state makes the work function decrease but the compressive state makes the work function increase, whereas the lateral strain state can disturb the work function strongly but the perpendicular state can hardly do so [37]. [8] used first principle to studies surface energies, work functions, and surface relaxations of low-index metallic surfaces, they result and comparison show that calculated values often do not quantitatively match experimental values. This may be understandable for the surface relaxations and surface energies, where experimental values can have large error but even for the work functions, neither local nor semi local functionals emerge as an accurate choice for every case. Work function and surface stability of tungsten-based Thermionic electron emission cathodes was studied by [38] the findings revealed consistent with transfer valency of Ba^{2+} and $O^{-2,}$ supercilious that some oxidation of work function occurred and then matching charge. For the (001), (011), (111), (211), and (310) surfaces, these steady Ba–O (Ba/O < 1) surfaces have low work functions of less than or equal to 2 eV. These results show that both low and high index surfaces might display a similar low work function and then could contribute substantially to the measured electron ejection [43]. Ab initio study of surface stress response to charging, was conducted by [9] the work function, surface stresses and coupling coefficient on Au surfaces using DFT reported by the authors is shown in table 2.1.

Table 2.1: Work function, surface stresses and coupling coefficient reported by [9].

Surface	**Stresses (Jm^{-2})**	**Work function (eV)**	**Coupling coefficient (V)**
Au (100)	2.723	5.56	−0.90
Au (110)	2.020	5.42	≈0
Au (111)	3.317	5.65	−1.86

[7] used density functional approach to examine the Surface energy and work function of FCC and BCC crystals, the results of the work functions with the surface crystallographic positioning revealed a good uniformity. for alkali metals, the work functions are increasing and, in the sequence, (110), (133), (311), (120), (100), (111). Also, for the similar crystal structure of BCC Nb, Mo, Ta, W transition metals the order is (110), (133), (120), (111), (311), (100). The work functions for FCC 3d, 4d and 5d transition metals likewise displayed a noticeable uniformity and ordered as (111), (100), (211), (123), (310), (110) [7].

[60] observed the surface relaxation, electronic work function and surface energy of BCC Li for (100), (110) and (111) surfaces computed using ab initio molecular dynamics procedures using local density approximation. The obtained relaxations for three-layer Li slabs are outer for the (100) and inner for the (110) and (111) surface layers. The outcomes display that the work function increases in the order (100) > (111) > (110) in the surface orientation. Moreover, the results revealed that the various energy quantities converge fast with increasing number of atomic layers [60]. Some theoretical results obtained by [7] as compared to experimental values of surface energy and work function reported by [7] for some metallic surfaces are shown in table 2.2.

Table 2.2: Surface energies and work function reported by [7] for some metals.

Surface	**Surface energy (Jm^{-2})**	**Experimental results**	**Work function (eV)**	**Experimental results**
Ag (100)	1.267	4.246	4.246	4.64
Ag (110)	1.350	1.26	4.059	4.52
Ag (111)	1.153	1.25	4.368	4.74
Ag (123)	1.382		4.138	
Ag (211)	1.302		4.238	
Ir (100)	3.492)		5.55	5.67
Ir (111)	2.775	3.00	5.497	5.76
Ir (123)	3.521		5.072	
Ir (211)	3.320		5.284	
Ir (310)	3.684		5.134	
Pt (100)	2.474		5.625	5.82 ± 0.15
Pt (110)	2.495		5.223	5.35 ± 0.05
Pt (111)	2.004	2.48	5.702	6.08 ± 0.15
Pt (123)	2.376		5.436	
Pt (211)	2.221		5.555	
Pt (310)	2.506		5.419	
Au (100)	1.359		5.071	5.22 ± 0.04
Au (110)	1.414		4.91	5.20 ± 0.04
Au (111)	1.137	1.50	5.110	5.26 ± 0.04

Au (123)	1.378		4.980	
Au (211)	1.293		5.01	
Au (210)	1.447		4.925	
Cu (100)	2.145		4.506	4.59
Cu (110)	2.192		4.272	4.48
Cu (111)	1.939	1.83	4.714	4.94
Cu (123)	2.244		4.35	
Cu (211)	2.096		4.453	
Cu (210)	2.279		4.258	
Ca (100)	0.529		2.758	
Ca (110)	0.635		2.813	
Ca (111)	0.548	0.502	2.936	2.87
Ca (123)	0.637		2.778	
Ca (211)	0.612		2.825	
Ca (310)	0.619		2.714	
Ba (100)	0.415		2.31	
Ba (110)	0.407	0.38	2.384	
Ba (111)	0.495		2.293	2.7
Ba (120)	0.446		2.346	
Ba (133)	0.466		2.341	
Ba (311)	0.471		2.327	

Density functional theory method was used by [61] to studies the surface energies and work functions for ten categories of Miller-indices surfaces of hexagonal metals for Be, Mg, Tc, Re, Ru, and Os. The results revealed that the metals in the same group have similar order in work functions and surface energies. The work functions of (0001), $01\bar{1}1$, and $10\bar{1}0$ surfaces are mostly larger than the work functions $(11\bar{2}1)$, $(11\bar{2}2)$, $(11\bar{2}3)$ and $(31\bar{4}0)$ surfaces [67]. Coupling coefficients for a number of low-index transition metal surfaces mainly of the 4d series have quantitatively determined and obtained negative values ranging from -0-3 V to -2.5 V[62]. Weigend et al. have executed first principles calculations for the charge-induced relaxation of Au cluster with 309 atoms containing (111) and (100) surfaces giving outward relaxation of the first atomic layer additional electrons. Furthermore, they proposed a phenomenological model which justifies the negative sign of and thus the increase of the surface stress upon negative charging as resulting from the transverse contraction in retort to the charge-induced outward relaxation of the top layer[63]. Common data available associated to electrocapillary coupling are for transition metal surfaces. Solely negative values have been testified for dissimilar clean transition metal surfaces both from theoretical and experimental methods [48]. A linear relation between the surface stress of a Au(111) cantilever and q in different electrolytes with a slope depending on the strength of adsorption of the employed anions was reported[64]. A good agreement of experimental values of the coupling coefficient, ς for (111)-textured Au electrodes of -2 V measured via cantilever bending and -1.9 V from potential strain response with a DFT calculations of the work function strain response for a planar Au(111) surface in vacuum, which yielded ς = -1.86 V[9, 53]. Comparable agreement is observed for Pt(111) and Pd(111) surfaces, where DFT values of-1.00 V (Pt) and -0.98 V (Pd) compare to -1.34 V and -1.31 V from electrochemical measurements of the potential-strain coupling in the capacitive regime using Dynamic Electro-Chemo-Mechanical

Analysis (DECMA) [48].

In the context of the phenomenological framework, a dependency of the materials variables on the state variables is permissible and indeed experiments reveal that the electrocapillary coupling coefficient is a function of the electrode potential $\varsigma = \varsigma(U)$[16, 53]. Electrosorption of Hydrogen on Pd is also characterized by a positive coupling coefficient of similar magnitude. Electrochemical experiments presented that the surface stress of Pd electrodes decreases during electrosorption of Hydrogen [11, 16]. The surface stress variation is quantitatively consistent with a continuum mechanics analysis of a misfitting solute atom in a superficial layer of a solid substrate yielding a value of $\varsigma = +1.2$ V [16]. This is compatible with $\varsigma = +1.4$ V obtained from cyclic voltammetry measurements of strained (pseudomorphic) layers and the DECMA result for potential-strain coupling of $\varsigma = 1{:}36$ V [48].

CHAPTER THREE

METHODOLOGY

3.1 Introduction

All calculations were performed using the Vienna Ab-initio Simulation Package (VASP) codes, and the projector-augmented wave (PAW) method was used [7, 71]. The calculation code has already been installed and available in the VASP library. for surface energy calculations, the electronic exchange-correlation potentials were described by the local density approximation (LDA) and for the work function calculations using the generalized gradient approximation of Perdew, Burke, and Ernzerh (GGA-PBE) functional [7,71]. The energy cut-off for the plane-waves of the system was set to 350 eV, the K-Point meshes were adjusted depending on the size of the surface modeled to provide well converged total energies [7]. The conjugate gradient minimization algorithm was employed for geometry optimizations, ensuring that the forces on each relaxed atom reached [71]. To get accurate results of the calculations we optimized the structure, kinetic energy cut – off (Ecut), K-Points and lattice parameter.

3.2 COMPUTATIONAL DETAILS

3.2.1 Kinetic energy cut-off (Ecut) optimization

The kinetic energy cut-off (ecut) optimization was done to limit the number plane waves with energy smaller than and/or equal to kinetic energy cutoff. This is required to computation efficiency while maintaining the accuracy of the computation result. In a periodic system, the plane wave is expressed by [66].

$$\Psi_k(r) = \frac{1}{\Omega}\sum_{G} c_k, G\, e^{i(k+G)r} \qquad (3.1)$$

With, G as a reciprocal lattice vector. This plane wave can be signified as a grid in the K-plane. The higher number of grid will make the calculation to be more precise but required long time for calculation, it is usually restricted by the cut-off energy unit, given by [72]

$$\frac{\hbar|k+G|^2}{2m} \leq E_{cut} \tag{3.2}$$

The parameter used in the INCAR file is Encut. In this study, the Encut value was varied in the range of 50-500 eV.

3.2.2 The K-point Optimization

The total energy and density calculations were perfectly performed for all values of **K** plane waves. Nevertheless, a finite number of **K** plane waves were considered. The Monkhorst-Pack mesh variation of $k_1 \times k_2 \times k_3$ was used limited Brillouin Zone (BZ) sampling from 1×1×1 to 21×21×21 for finding the best convergence with total energy value.

3.2.3 Lattice Parameters Optimization

Optimization of the Structural was done by optimizing the crystal lattice constant[66]. In this study, a face centered cubic crystal structure of Au was used. The lattice constant optimization was carried out by giving the initial lattice constant (a_0) smaller value which is less than the expected value. The calculations were reiterated and at the end of each stage we found the total energy (E) corresponding to the assumed lattice constant. The iteration continued until a minimum total energy is found which convergences the lattice parameters.

3.2.4 Surface Optimization

Surface optimization is characterized as the percent variation Δd_{ij} of the spacing among layers *i* and *j* against the equilibrium layer spacing d_0 [8].

$$\Delta d_{ij} = \frac{d_{ij} - d_0}{d_0} \tag{3.3}$$

Where d_0 is the bulk interlayer spacing for the particular surface orientation. optimization of the top layer is usually most noticeable, there can be substantial multilayer optimizations spreading deep into the crystal, especially for the more open surfaces [11]. In this study the optimization was conducted by taking three different doped surfaces of 14, 16 and 18 layers to obtained the most converge surface.

3.3 Implementation of strain

The different components of the deformation of the strained surface slabs are considered. The work function strain response parameter was determined using the equation given by

$$\varsigma = \frac{dW}{de} \tag{3.4}$$

the surface slab was subjected to isotropic in-plane strain. The parameter e measures the relative change in surface area A, $e = \frac{\delta A}{A_0}$ where, A_0 is the area of the two-dimensional surface unit cell of the unstrained slab. Thus, in-plane strain is imposed by scaling the in-plane lattice vectors by a factor of $\sqrt{1 + e}$. While in experiment purely elastic strain can only be achieved at very small strain amplitudes of about 10^{-3}. This kind of strain values would be too small to resolve the corresponding change in the work function, meanwhile DFT calculations do not include any plastic distortion, it is possible to apply larger strain values [11]. The main interest of this study is on the first order change of the work function with strain values. We applied strain from -0.04 up to 0.04

because it is usually small and sufficient to give an approximately linear relation between W and e. Single point calculations were performed for each strain applied to determine the wave function corresponding to each strain. Vaspkit was used to run the calculation. The vaspkit calculate the wave function by taking the Fermi and the vacuum potential in accordance with equation (2.4). The results obtained were linearly fitted and the coupling coefficient was determined from the fitting equation. The coupling coefficient was then found as the slope of a linear fit to the data of work function (W) against strain (e) graph.

3.4 Calculation of the Surface stress

The following formula represents the shift in a system's total energy as the deformation tensor changes [67]:

$$\delta E = \int \sum_{ij} \sigma_{ij}(r)\delta\epsilon_{ij}dr \qquad (3.5)$$

where at point **r** = (*x*,*y*,*z*), $\sigma_{ij}(r)$ is the stress tensor. Assuming periodicity in x and y directions and by using a slab geometry, we have

$$\delta E = A\int_{\frac{-d}{2}}^{\frac{d}{2}} \sum_{ij} \tau_{ij}(z)\delta\epsilon_{ij}dz \qquad (3.6)$$

Here z is perpendicular to the surface of the slab, the slab's thickness is denoted by d, its surface area is represented by A, and the $\tau_{ij}(z)$are the components of the ‘‘slab’’ stress tensor introduced as

$$\tau_{ij}(z) = \frac{1}{A}\int \sigma_{ij}(r)dxdy \qquad (3.7)$$

The surface stress tensor is defined from $\tau_{ij}(z)$ [68] by

$$\tau_{ij}^{(s)} = \int \left[\tau_{ij}(z) - \tau_{ij}^{(b)}\right] dz \tag{3.8}$$

Where $\tau_{ij}^{(b)}$represents the slab stress tensor value in the bulk region (far from the surface). Equation (3.6) can be divided into two segments with respect to the surface stress tensor as

$$\delta E = 2\delta E^{(S)} + \delta E^{(b)} = 2A \sum_{ij} \tau_{ij}^{(s)} \delta\epsilon_{ij} + Ad \sum_{ij} \tau_{ij}^{(b)} \delta\epsilon_{ij} \tag{3.9}$$

The slab's two surface facets give rise to the factor 2. As a result, there is a relationship between the change in the deformation tensor $\delta\epsilon_{ij}$ and the changes in bulk $\delta E^{(b)}$ and slab $\delta E^{(S)}$ energies.

$$\delta E^{(s)} = \frac{1}{2}\left[\delta E - \delta E^{(b)}\right] = A \sum_{ij} \tau_{ij}^{(s)} \delta\epsilon_{ij} \tag{3.10}$$

Furthermore,

$$\tau_{ij}^{(s)} = \frac{1}{A} \frac{\delta E^{(S)}}{\delta\epsilon_{ij}} \tag{3.11}$$

We can write (3.11) by substituting the relation $E^{(S)} = A\gamma$,

$$\tau_{ij}^{(s)} = \gamma\delta_{ij} + \frac{\delta\gamma}{\delta\epsilon_{ij}} \tag{3.12}$$

Where γ is the surface energy defined as the reversible work per unit area to create a surface.

Where $\frac{\delta\gamma}{\delta\epsilon_{ij}}$ is the residual surface stress. Equation (3.12) is known as Shuttleworth equation, showing that the surface stress is the reversible work per area to stretch the surface elastically.

In this work equation (3.10) was used to compute the surface stress. Slab geometry was used in the calculation, and the third lattice vector—which establishes the layer distance—is maintained fixed while the lattice vectors extending in the surface plane are extended by ϵ during the "stretching"deformation. The shape of the deformation tensor for this distortion is as follows.

$$\epsilon_{ij} = \begin{bmatrix} \epsilon & 0 & 0 \\ 0 & \epsilon & 0 \\ 0 & 0 & \epsilon \end{bmatrix}$$

The change in the energies $\delta E^{(b)}$ and δE are given as a function of ϵ. Various values of ϵ were used to calculate the total energies of the slab and bulk systems of Au (111). The noise from the calculated mesh points was reduced by using a fitting equation in the form of a polynomial approximation.

$$\delta\epsilon \approx c_0 + c_1\epsilon + c_2\epsilon^2 + \cdots \quad (3.13)$$

Consequently, the linear coefficients of the slab and bulk energies, can be used to find the surface stress by using equation (3.14)

$$\tau^{(s)} = \frac{c_1^{(s)} - c_1^{(b)}}{2A} \quad (3.14)$$

The area of the two-dimensional unit cell on (111) surface is $A = \left(\frac{\sqrt{3}}{4}\right) a^2$, where a is the theoretical (computed) lattice constant.

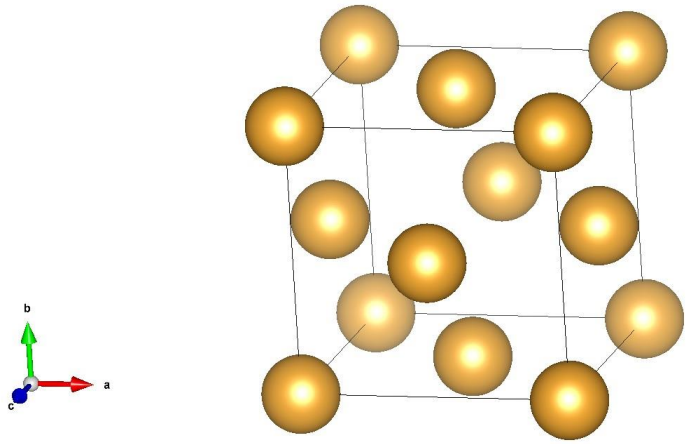

Figure 3.1: Au (100) conventional unit cell

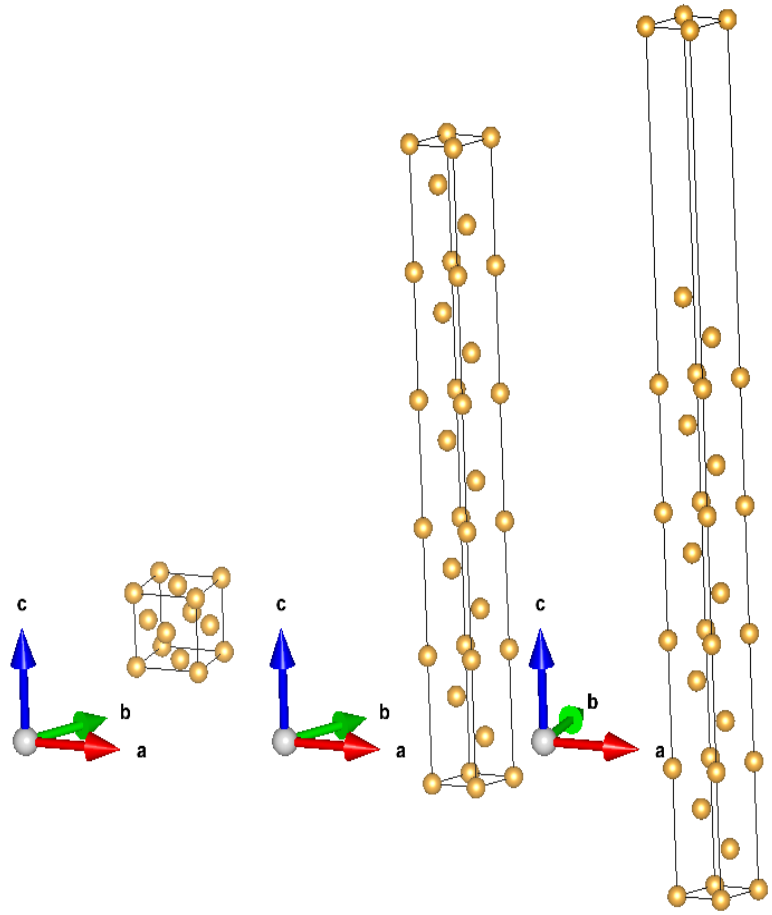

Figure 3.2: Au (111) bulk and slab super cells.

CHAPTER FOUR

RESULTS AND DISCUSSION

The results obtained are presented in this chapter and discuss accordingly.

4.1 Results from Parameters Optimization Calculation

The results obtained of the total energy convergence with the energy cutoff are presented in table 4.1.

Table 4.1: Total energy convergence with energy cut-off.

Energy cutoff (eV)	Total Energy (eV)
100	45.22508183
150	-14.60215037
200	-17.25138238
250	-17.59220988
300	-17.56225425
350	-17.53451466
400	-17.53472539
450	-17.53509303
500	-17.53403554

From table 4.1 it was observed that as the energy cutoff increases the total energy decreases and the energies converges as the energy cutoff approaches 350 eV. The highest value of the total energy is found when the energy cut-off is lowest. The optimization result of the energy cutoff parameter for the Au (111) calculation in the range of 50 eV to 500 eV is displayed in figure 4.1.

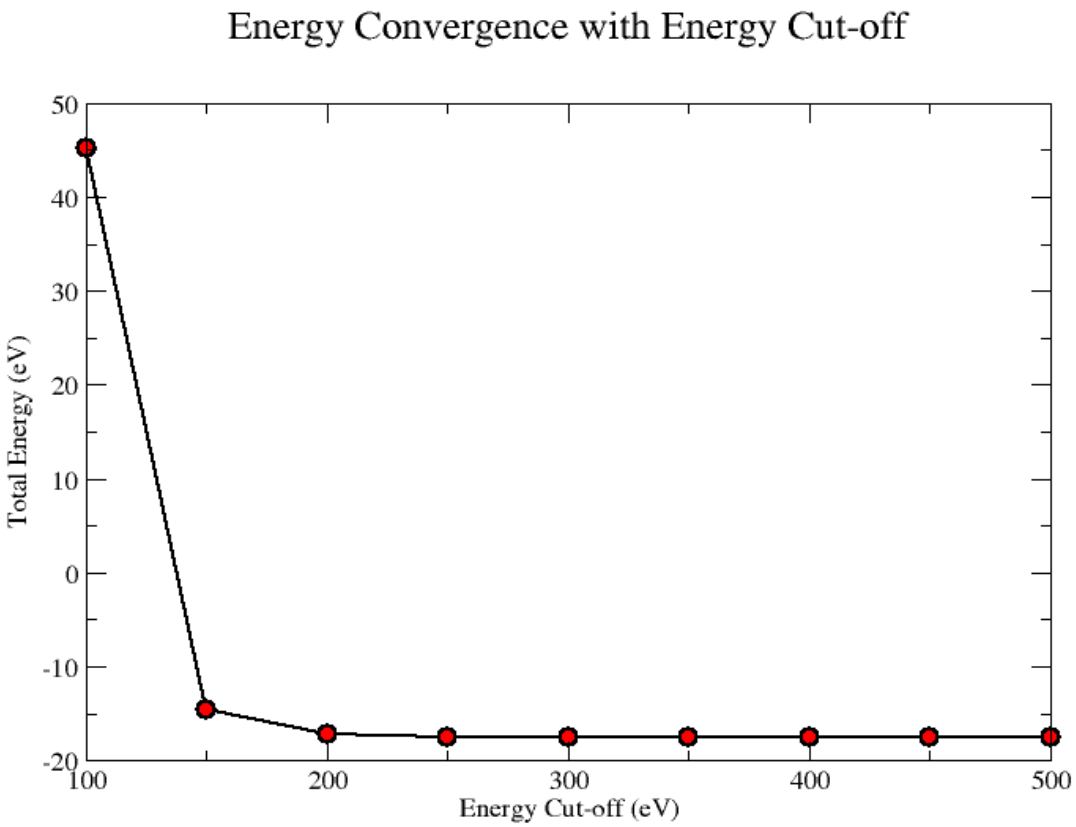

Figure 4.1: Plot showing the total energy plotted against the energy cut – off.

The value of the total energy decreases as the energy cut – off increases. However, as the value of the energy cut – off approaches 300 eV to 500 eV the value of the total energy does not change significantly. Hence, the value of 350 eV was used as the kinetic energy cut-off in the calculations. The results obtained for the total energy convergence with Kpoints are presented in table 4.2.

Table 4.2: Results of K points convergence with total energy

K POINTS	TOTAL ENERGY (eV)
01	-4.48920759
03	-17.08391414
05	-17.40967212
07	-17.50700164
09	-17.54400416
11	-17.54322620
13	-17.53895503
15	-17.53720641
17	-17.53502475
19	-17.53459073
21	-17.53451466

From table 4.2 it was observed that the total energy decreases with increases in the number of K points in the mesh grid and converges as the K points approaches 9×9×9. In the K Points values optimization, the results for grid variations from 1to 21 are shown figure 4.2.

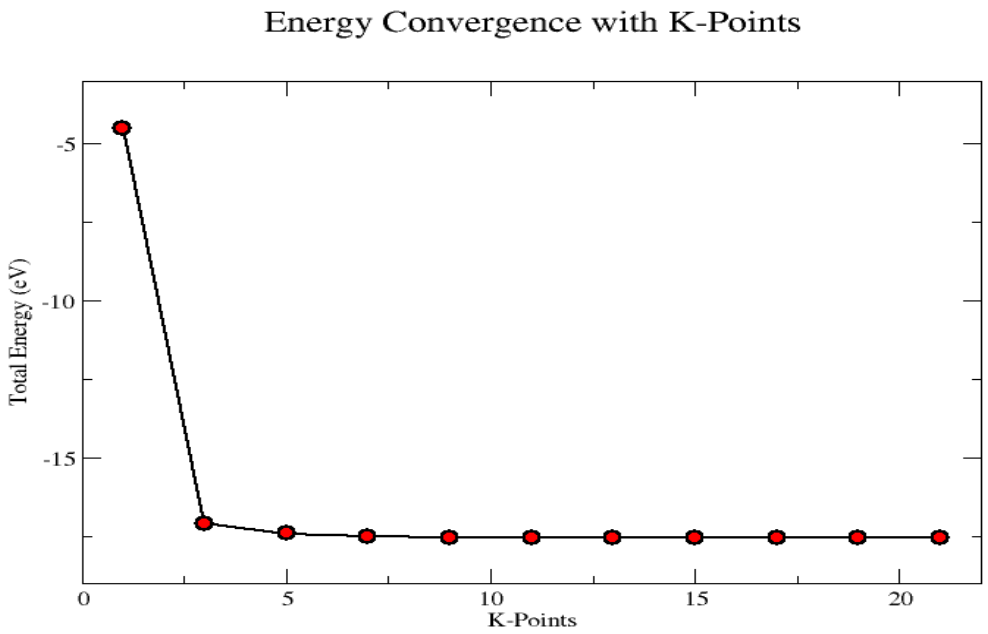

Figure 4.2: Plot showing the total energy plotted against the K-Points

Figure 4.2 presents value of the total energy generated for each grid. The highest total energy obtained is generated on the grid of 1×1×1. The total energy value varies but comparative constant for grid size larger than 11. Consequently, the grid size of 9×9×9 will be used for further calculation. This value of the K-Point is precisely sufficient to obtain the total energy. However, it requires denser points for electronic structure calculation to get the smoother curve. In this work, K-Point of the form 9×9×1 was used. The results obtained for the total energy convergence with lattice parameters are displayed in table 4.3.

Table 4.3: Results of total energy convergence with lattice parameters.

Lattice Parameter (Å)	**Total energy (eV)**
3.94	-17.497737
3.96	-17.604893
3.98	-17.688594
4.00	-17.749758
4.02	-17.790004
4.04	-17.810604
4.06	-17.813167
4.08	-17.798583
4.10	-17.767734
4.12	-17.722286
4.14	-17.663130
4.16	-17.590855
4.18	-17.506732
4.20	-17.411614
4.21	-17.360339

From table 4.3 the experimental lattice constant parameter was used to get the calculated lattice parameter by varying the lattice parameter around the minimum value of the experimental lattice parameter. The results obtained in the lattice parameter optimization is shown in figure 4.3.

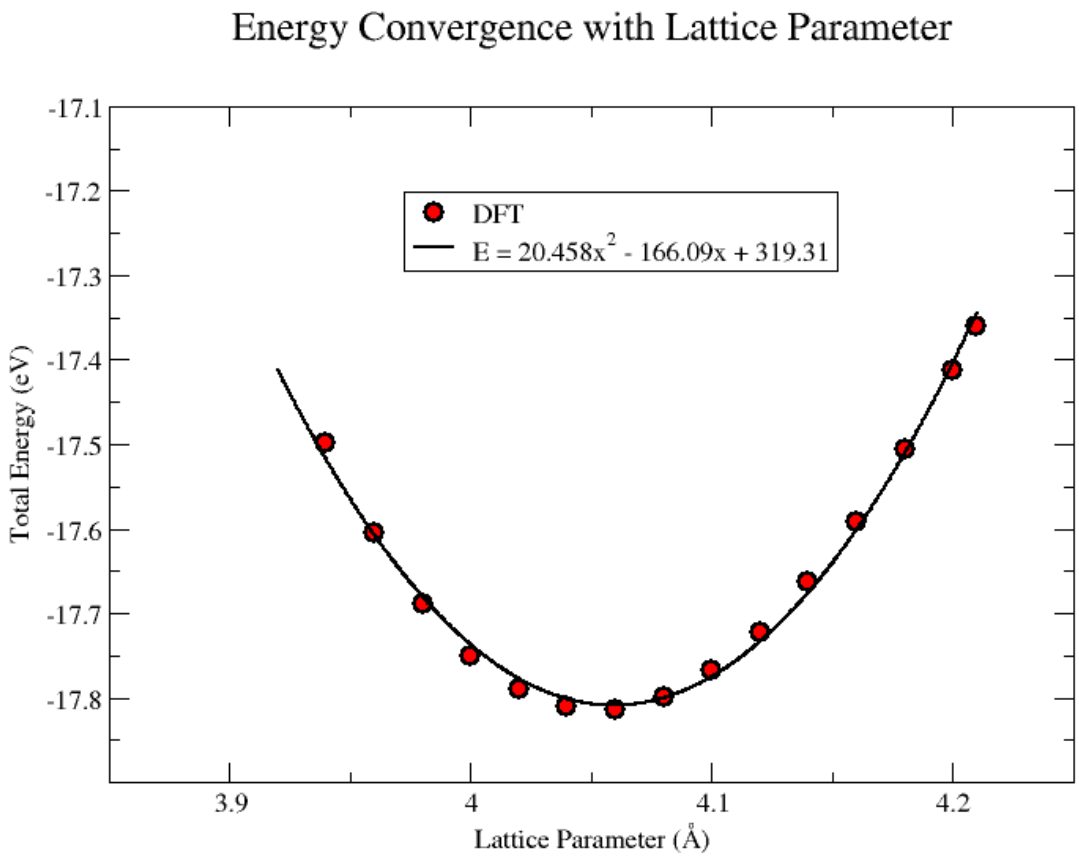

Figure 4.3: Plot showing the total energy plotted against lattice parameter.

Figure 4.3 show a plot of the total energy values versus the lattice parameters of the Au crystal structure which was used to determine the minimum total energy of the crystal. The lattice constant with the minimum total energy was found to be the theoretical lattice constant obtained from the DFT calculation. In experimental literatures value of the lattice constant of Au is observed to be at 4.07825 Å and a theoretical value of 4.025 Å [3]. A second order polynomial of quadratic form was used to fit the data and the fitting equation obtained is given as

$$E = 20.458x^{2} - 166.09x + 319.31 \quad (4.1)$$

Where the coefficient x in equation (4.1) is the lattice constant.

The lattice constant in equation (4.1) can be found by differentiating equation (4.1) and hence,

$$\frac{dE}{dx} = 40.916x - 166.09 \quad (4.2)$$

To get the lattice constant the energy most be minimum, this was achieved by equating equation (4.2) to zero and the lattice constant was found to be 4.059 Å. In this work the lattice constant obtained from the DFT calculation 4.059 Å was used.

4.2 Result from the Computation of Surface Energy

The results obtained for the computation of surface energy by observing the variation of energy per unit cell with slab thickness (number of layers) are displayed table 4.4

Table 4.4: Result for the computation of surface energy.

Number of Layers	Energy/unit cell (eV)
03	-12.27861662
05	-21.18551068
07	-30.13757049
09	-39.07751259
11	-47.98179155
13	-56.91049256
15	-65.82791259

From table 4.4 it was observed that the energy per unit cell of the slab decreases as the number of layers (slab thickness) increases. The results in shown in table 4.4 is displayed in figure 4.

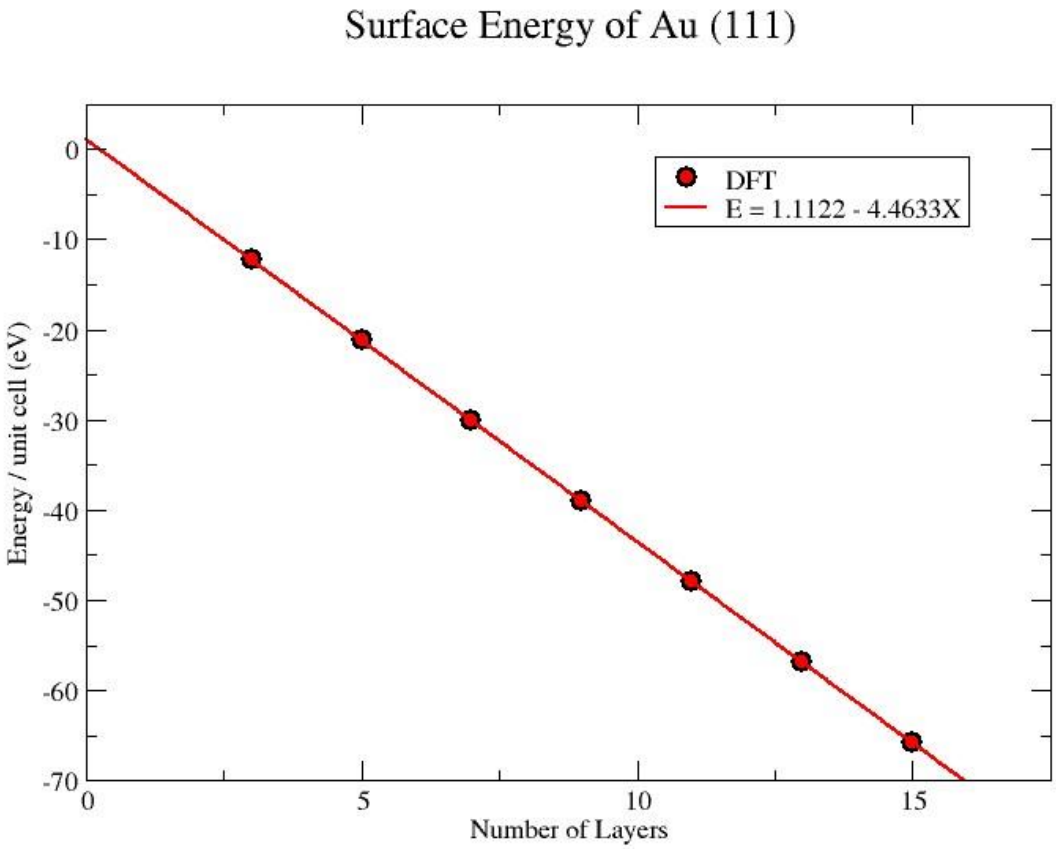

Figure 4.4: Plot showing the total energy per unit cell against number of layers.

In order to find the surface energy of Au (111) the data of the result represented in figure 4.4 was fitted linearly and the following equation is obtained

$$y = 1.1122 - 4.4633x \qquad (4.3)$$

By comparing equation (4.3) with equation (2.2) the surface energy of Au (111) was found to be

$\sigma = \frac{1.1122}{2} = 0.5561\ \text{eVÅ}^{-1}$

4.3 Results from the Computation of Surface Stress

The results obtained for the computation of surface stress for both the bulk and slab are displayed in table 4.5.

Table 4.5: Results of applied strain and energy for bulk and slab.

Strain	**Energy (eV)**	
	Bulk	**Slab**
-0.04	-66.62610839	-43.59514729
-0.03	-66.73687264	-43.61421784
-0.02	-66.80625553	-43.61573833
-0.01	-66.83719958	-43.60130997
0.00	-66.83388768	-43.57303717
0.01	-66.79747373	-43.53080637
0.02	-66.73003876	-43.47498722
0.03	-66.63635208	-43.40770457
0.04	-66.51622105	-43.32851411

In table 4.5 the strain was applied to the bulk and slab for deformation along the x – axis. It was observed that as the strain applied was increased the energy of both the bulk and slab reduced. The results presented in table 4.5 were represented graphically as shown in figure 4.5a and 4.5b

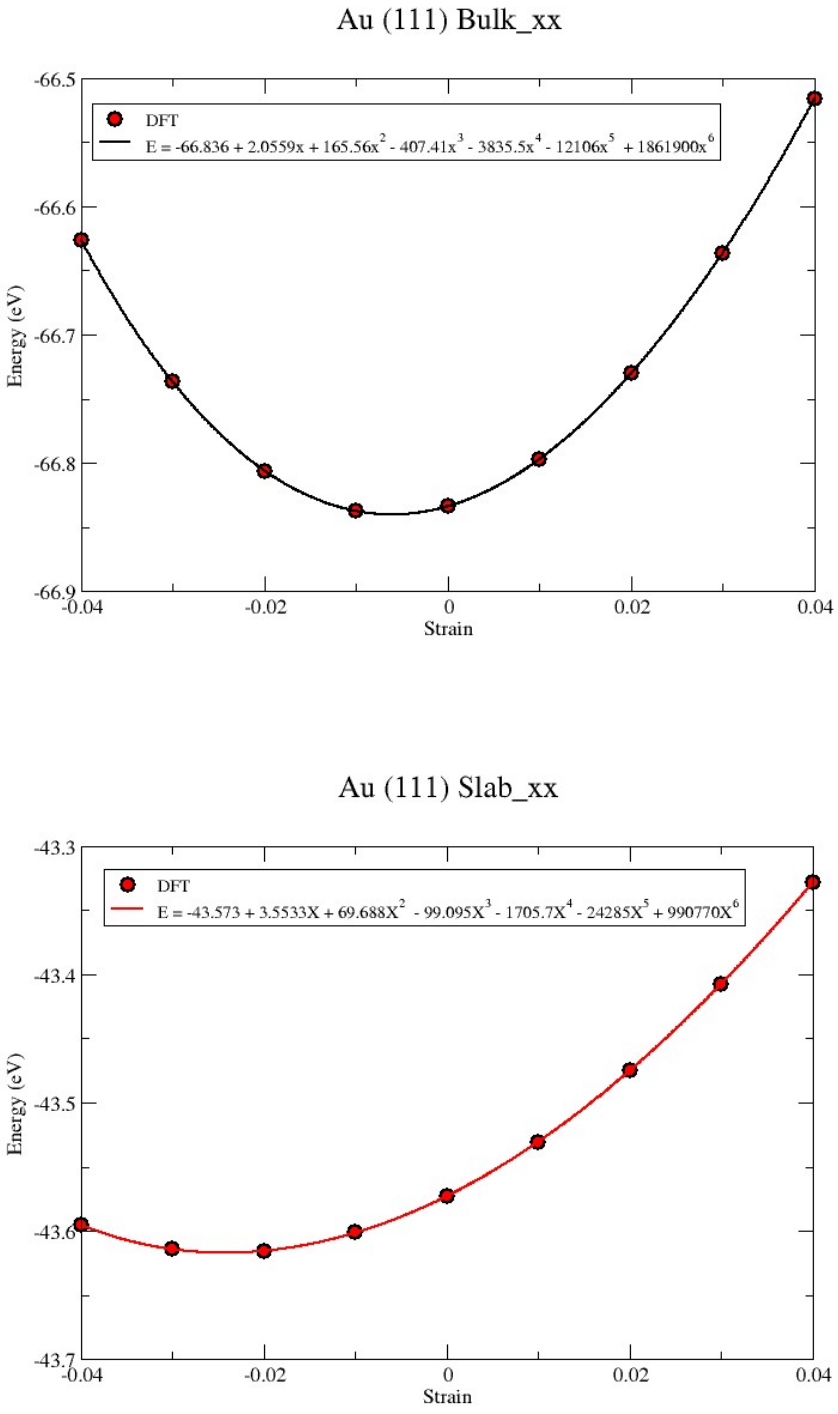

Figure 4.5 (a): Plot showing the total energy against the strain applied for bulk deformation along x-axis, **(b)** Plot showing the total energy against the strain applied for slab deformation along x-axis.

Polynomial fitting was used to find the energy changes $E_{xx}^{(b)}$ and $E_{xx}^{(s)}$ for the bulk and slab respective as a result of deformation. The fitting equations found to be;

$$\delta E_{xx}^{(b)} = -66.836 + 2.0559x + 165.56x^2 - 407.41x^3 - 3835.5x^4 - 12106x^5 + 1861900x^6 \quad (4.4)$$

$$\delta E_{xx}^{(s)} = -43.573 + 3.5533x + 69.688x^2 - 99.095x^3 - 1705.7x^4 - 24285x^5 + 990770x^6 \quad (4.5)$$

The coefficients in equation (4.4) and (4.5) was found by comparing these equations with equation (3.3) and equation (3.4) was used to find the surface stress as follows;

$c_{1xx}^{(b)} = 2.0559\ eV$, $c_{1xx}^{(s)} = 3.5533\ eV$, and substituting these values in equation (3.14) the surface stress along x – axis reads;

$$\tau_{xx}^{(s)} = \frac{c_{1xx}^{(s)} - c_{1xx}^{(b)}}{2A} = \frac{3.5533 - 2.0559}{2 \times 4.1189} \frac{eV}{\text{Å}^2} = 0.18177 \frac{eV}{\text{Å}^2} = 2.912\ \frac{J}{m^2}$$

4.3 Result from the Computation of Coupling Coefficient

The results obtained for the computation of coupling coefficient are displayed in table 4.6.

Table 4.6: Variation of applied strain with work function.

Strain	Work function (eV)
-0.04	-5.616
-0.03	-5.606
-0.02	-5.597
-0.01	-5.586
0.00	-5.575
0.01	-5.564

0.02	-5.553
0.03	-5.539
0.04	-5.522

It was observed that in table 4.6, work function decreased as the applied strain is increased. The results presented in table 4.6 were represented graphically as shown in figure 4.7.

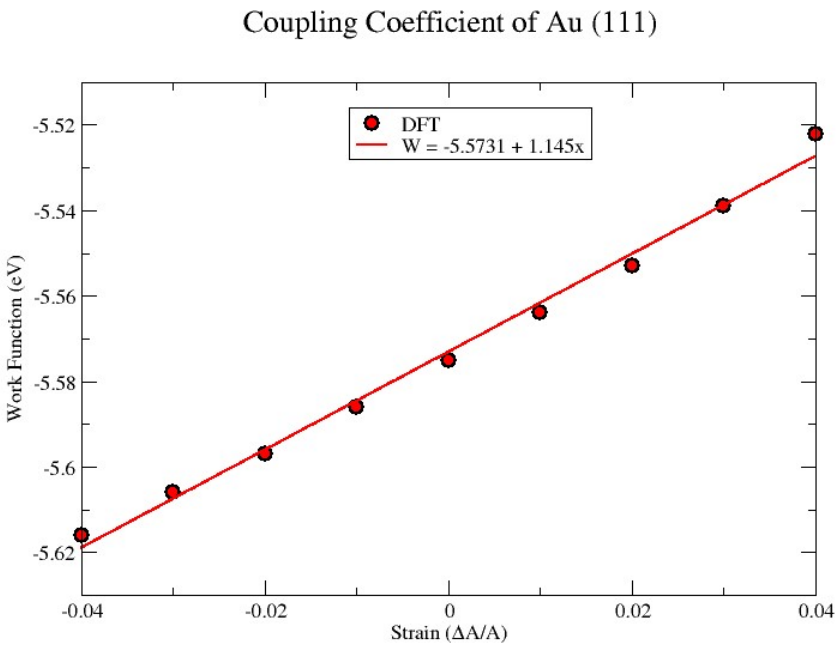

Figure 4.6: Plot showing the variation of strain applied with work function.

A linear fit was used for fitting the results presented and the fitting equation obtained is

$$W = 1.145x - 5.5731 \quad (4.6)$$

The coefficient x, in equation (4.6) denotes the strains applied during the deformation. The coupling coefficient ς, by the slope of the graph of work function against strain and hence, in accordance with equation (4.6) the coupling coefficient is found to be $\varsigma = 1.145\ eV$. This result shows that the calculated coupling coefficient is positive.

CHAPTER FIVE

CONCLUSION AND RECOMMENDATION

5.1 CONCLUSION

In this study, ab initio calculations were executed to ascertain diverse material properties, adopting established practices. A systematic examination of the convergence of these properties including cutoff energy, K-point sampling, and lattice parameter was conducted to guarantee the reliability and consistency of the results.

The findings of this investigation reveal that the Au (111) surface possesses a surface energy of 0.5561 $eV\text{Å}^{-1}$, a surface stress of 0.18177 $eV\text{Å}^{-2}$, and a coupling coefficient of 1.145 eV, hold significant implications for surface stability. The surface energy, indicative of the energy required to form a unit area of the surface, is a crucial metric for understanding the thermodynamic stability of a material. In the case of Au (111), the obtained surface energy provides insights into the energetics governing the stability of its exposed surface. A lower surface energy generally implies greater stability, suggesting that Au (111) is expected to exhibit favorable stability characteristics. Surface stress, denoting the force per unit length acting on the boundary of a crystal surface, is an essential factor influencing the mechanical and thermodynamic behavior of materials. The calculated surface stress of 0.18177 $eV\text{Å}^{-2}$ for Au (111) highlights its response to external forces and perturbations. This parameter is indicative of the material's resistance to deformation and its ability to maintain structural integrity under stress conditions.

The coupling coefficient, representing the strength of interaction between atoms in adjacent layers of a crystal lattice, is a crucial factor influencing the overall stability of a material. The determined coupling coefficient of 1.145 eV for Au (111) signifies the cohesive forces within the crystal structure, shedding light on its bonding characteristics and potential applications in various

contexts. Lastly, the comprehensive ab initio calculations performed in this study provide valuable insights into the material properties of Au (111). The obtained results, including surface energy, surface stress, and coupling coefficient, contribute to our understanding of the surface stability of this material, with potential implications for its applications in diverse fields, such as catalysis, materials science, and nanotechnology.

5.2 RECOMMENDATION

For future investigations, it is recommended that studies explore high Miller index geometries to gain deeper insights into their distinct surface behaviors. Exploring these higher index surfaces is imperative for a more comprehensive understanding of the material's surface characteristics and their potential applications in various fields. Furthermore, future research endeavors should focus on unraveling the impact of impurities on crucial surface properties, including surface energy, surface stress, and coupling coefficient. Investigating both low and high index surfaces in the presence of impurities is essential for elucidating the material's response to external influences and its stability under real-world conditions. Such an exploration would contribute significantly to refining our understanding of the material's behavior and guide the development of tailored applications in areas such as catalysis, materials engineering, and nanotechnology.

In essence, by extending investigations to encompass high Miller index geometries and incorporating impurity effects, future studies can provide a more nuanced and comprehensive perspective on the surface characteristics of the material. This expanded knowledge base will not only deepen our understanding of its fundamental properties but also pave the way for the development of advanced materials with enhanced functionalities and tailored applications.

REFERENCES

[1] N. M. Stuart and K. Sohlberg, "asymmetric slab models †," 2023, doi: 10.1039/d2cp04460a.

[2] J. F. Dobson, "Metallic Surfaces and Density Functional Theory. In: Gross, E.K.U., Dreizler, R.M. (eds) Density Functional," *NATO ASI Ser.*, vol. 337, 1995, [Online]. Available: https://doi.org/10.1007/978-1-4757-9975-0_16

[3] R. J. Needs, "Calculations of the Surface Stress Tensor at Aluminum (111) and (110) Surfaces.pdf."

[4] H. Search, C. Journals, A. Contact, M. Iopscience, and I. P. Address, "Surface relaxation and stress for 5d transition metals," vol. 095007, doi: 10.1088/0953-8984/21/9/095007.

[5] Tyson W.R. and M. W.A., "Surface Free Energies of Solid Metals Estimation from Liquid Surface Tension Measurements," *Surf. Sci.*, vol. 62, pp. 267–276, 1977.

[6] P. Chen, Y. Gao, and M. R. Castell, "Experimental determination of the {111}/{001} surface energy ratio for Pd crystals," *Appl. Phys. Lett.*, vol. 117, no. 10, pp. 1–5, 2020, doi: 10.1063/5.0022879.

[7] J. Wang and S. Wang, "Surface Science Surface energy and work function of fcc and bcc crystals : Density functional study," *Surf. Sci.*, vol. 630, pp. 216–224, 2014, doi: 10.1016/j.susc.2014.08.017.

[8] N. E. Singh-miller and N. Marzari, "Surface energies , work functions , and surface relaxations of low-index metallic surfaces from first principles," pp. 1–9, 2009, doi: 10.1103/PhysRevB.80.235407.

[9] M. N. Y. Umeno, C. Els¨asser, B. Meyer, P. Gumbsch and and F. E. J. Weissm¨uller, "Ab initio study of surface stress response to charging Ab initio study of surface stress response

to charging," 2007, doi: 10.1209/0295-5075/78/13001.

[10] D. Kramer, R. N. Viswanath, and J. Weissmüller, "Surface-stress induced macroscopic bending of nanoporous gold cantilevers," *Nano Lett.*, vol. 4, no. 5, pp. 793–796, 2004, doi: 10.1021/nl049927d.

[11] A. Michl, "Coupling between electronic , mechanical and vibrational properties of clean and adsorbate-covered metal surfaces – a first-principles study," 2017.

[12] Y. Wu and Y. Yu, "Author ' s Accepted Manuscript," *Energy Storage Mater.*, 2018, doi: 10.1016/j.ensm.2018.05.026.

[13] L. E. Y. D. E. Adquisiciones *et al.*, "No 主観的健康感を中心とした在宅高齢者における 健康関連指標に関する共分散構造分析Title," *Duke Law J.*, vol. 1, no. 1, 2019.

[14] H. Jin, X. Wang, S. Parida, K. Wang, and M. Seo, "Nanoporous Au - Pt Alloys As Large Strain Electrochemical Actuators," pp. 187–194, 2010, doi: 10.1021/nl903262b.

[15] S. M. and M. M. M. Hakamada, "Electrochemical actuation of nanoporous Ni in NaOH solution.," *Mater. Lett.*, vol. 70, pp. 132–134, 2012.

[16] R. Viswanath and J. Weissmuller, "Electrocapillary coupling coefficients for hydrogen electrosorption on palladium," *Acta Mater.*, vol. 61, pp. 6301–6309, 2013.

[17] R. Viswanath and J. Weissmuller, "Adsorbate effects on the surface stress-charge response of platinum electrodes," *Electrochim. Acta*, vol. 2757, no. 53, 2018.

[18] Q. D. and J. Weissm uller, "Electrocapillary Coupling during Electrosorption.," *Langmuir 30*, vol. 30, pp. 10522–10530, 2014.

[19] R. Podloucky and J. Redinger, "Density functional theory study of structural and

thermodynamical stabilities of ferromagnetic MnX (X = P , As , Sb , Bi) compounds".

[20] X. Yang, M. Yang, B. Pang, M. Vara, Y. Xia, and U. States, "Gold Nanomaterials at Work in Biomedicine," 2015, doi: 10.1021/acs.chemrev.5b00193.

[21] doi:10. 1038/495s2. Savage, N., "Resources: Mine, all mine!," *Nature,* vol. 495, no. 7440, pp. 52–53, 2013, [Online]. Available: doi: 10.1038/495S2a

[22] R. Meyer, C. Lemire, S. K. Shaikhutdinov, and H. Freund, "Surface Chemistry of Catalysis by Gold *," no. 30, 2004.

[23] M. Haruta and M. Daté, "Advances in the catalysis of Au nanoparticles," *Appl. Catal. A Gen.*, vol. 222, no. 1–2, pp. 427–437, 2001, doi: 10.1016/S0926-860X(01)00847-X.

[24] M. Haruta, "Novel catalysis of gold deposited on metal oxides," *Catal. Surv. from Japan*, vol. 1, no. 1, pp. 61–73, 1997, doi: 10.1023/A:1019068728295.

[25] and V. B. Rohul H. Adnan, Gunther G. Andersson, Matthew I.J. Polson, Gregory F. Metha and Golovko, "Factors influencing the catalytic oxidation of benzyl alcohol using supported phosphine-capped gold nanoparticles," *Catal. Sci. Technol.*.

[26] J. Zhang and X. Jiang, "Chemical Science," 2020, doi: 10.1039/c9sc06497d.

[27] B. Nkosi, M. D. Adams, N. J. Coville, and G. J. Hutchings, "Hydrochlorination of acetylene using carbon-supported gold catalysts: A study of catalyst reactivation," *J. Catal.*, vol. 128, no. 2, pp. 378–386, 1991, doi: 10.1016/0021-9517(91)90296-G.

[28] and X. C. Wen Zhou, Xia Gao, Dingbin Liu, "Gold Nanoparticles for In Vitro Diagnostics," *Chem. Rev.*, 2015, [Online]. Available: https://doi.org/10.1021/acs.chemrev.5b00100

[29] C. Tao, "No TitleAntimicrobial activity and toxicity of gold nanoparticles: research progress, challenges and prospects," *Lett. Appl. Microbiol.*, vol. 67, pp. 537–543., 2018.

[30] G. J. Hutchings, “Catalysis by Gold: Recent Advances in Oxidation Reactions,” *Nanotechnol. Catal.*, pp. 39–54, 2007, doi: 10.1007/978-0-387-34688-5_4.

[31] J. L. F. Da Silva, C. Stampfl, and M. Scheffler, “Converged properties of clean metal surfaces by all-electron first-principles calculations,” *Surf. Sci.*, vol. 600, no. 3, pp. 703–715, 2006, doi: 10.1016/j.susc.2005.12.008.

[32] J. C. Boettger, “Nonconvergence of surface energies obtained from thin-film calculations,” *Phys. Rev.*, vol. 49, no. 16798, 1994.

[33] V. F. and M. Methfessel, “Extracting convergent surface energies from slab calculations,” *J. Phys. Condens. Matter*, vol. 8, no. 36, 1996, [Online]. Available: DOI 10.1088/0953-8984/8/36/005

[34] J. Weissmüller and J. W. Cahn, “Mean stresses in microstructures due to interface stresses: A generalization of a capillary equation for solids,” *Acta Mater.*, vol. 45, no. 5, pp. 1899–1906, 1997, doi: 10.1016/S1359-6454(96)00314-X.

[35] K. Gall, J. Diao, and M. L. Dunn, “The strength of gold nanowires,” *Nano Lett.*, vol. 4, no. 12, pp. 2431–2436, 2004, doi: 10.1021/nl048456s.

[36] O. C. Olawole, D. De, O. F. Olawole, and R. Lamba, “Progress in the experimental and computational methods of work function evaluation of materials : A review Heliyon Progress in the experimental and computational methods of work function evaluation of materials : A review,” no. October, 2022, doi: 10.1016/j.heliyon.2022.e11030.

[37] X. F. Wang, W. Li, J. G. Lin, and Y. Xiao, “Electronic work function of the Cu (100) surface under different strain states,” vol. 89, no. March, pp. 1–6, 2010, doi: 10.1209/0295-5075/89/66004.

[38] R. Jacobs, D. Morgan, J. Booske, R. Jacobs, D. Morgan, and J. Booske, “Work function and surface stability of tungsten-based thermionic electron emission cathodes Work function and surface stability of tungsten-based thermionic electron emission cathodes,” vol. 116105, 2017.

[39] M. V Strikha and A. Goriachko, “Surfaces with Lowered Electron Work Function : Problems of Their Creation and Theoretical Description . A Review WORK FUNCTION : PROBLEMS OF THEIR CREATION,” no. October, 2023, doi: 10.15407/ujpe68.8.549.

[40] S. H. T. Durakiewicz, J. Sikora, “T. Durakiewicz, J. Sikora, S. Halas,” *Vacuum*, vol. 80, no. 8, 2006.

[41] T. D. S. Halas, “Is work function a surface or a bulk property?,” *Vacuum*, vol. 85, pp. 486–488, 2010.

[42] K. I. I. & V. A. Korol’kov, “Temperature Dependence of the Work Function of Metals and Binary Alloys,” *Inorg. Mater.*, vol. 37, pp. 567–572, 2001.

[43] H. T. H. Lu, Z. Liu, X. Yan, D. Li, L. Parent, “Electron work function-a promising guiding parameter for material design,” *Sci. Rep.*, vol. 6, pp. 1–11, 2016.

[44] H. Y. I. Brodie, S.H. Chou, “A general phenomenological model for work func-tion,” *Surf. Sci.*, vol. 625, pp. 112–118, 2014.

[45] H. Lu and D. Li, “Correlation between the electron work function of metals and their bulk moduli, thermal expansion and heat capacity via the Lennard-Jones potential,” *Phys. Status Solidi Basic Res.*, vol. 251, no. 4, pp. 815–820, 2014, doi: 10.1002/pssb.201350017.

[46] D. Y. L. Y. Li, “Experimental studies on relationships between the electron work function, adhesion, and friction for 3d transition metals,” *J. Appl. Phys.*, vol. 95, p. 7961, 2004.

[47] N. D. L. and W. Kohn, “Theory of Metal Surfaces: Work function.,” *Phys. Rev*, vol. B 3, p. 1215, 1971.

[48] Q. Deng and J. Weissmüller, “Electrocapillary coupling during electrosorption,” *Langmuir*, vol. 30, no. 34, pp. 10522–10530, 2014, doi: 10.1021/la501353g.

[49] V. Shibayama, T., Dorn, C., K., Vladimir, C., Bachurin, D., V., Stihl, C., Vladimirov, P., “Beryllium and its Alloys as Neutron Multiplying Materials,” *Compr. Nucl. Mater. 2nd Ed.*, 2009, [Online]. Available: doi:10.1016/B978-0-12-803581-8.11673-X

[50] N. Lee, J., *Computational materials science: an introduction*, Second. Boca Raton: CRC Press, Taylor & Francis, 2017.

[51] F. Paquin, J. Rivnay, A. Salleo, N. Stingelin, and C. Silva, “Multi-phase semicrystalline microstructures drive exciton dissociation in neat plastic semiconductors,” *J. Mater. Chem. C*, vol. 3, pp. 10715–10722, 2015, doi: 10.1039/b000000x.

[52] A. Ullah, “DFT a practical approach”.

[53] R. Aamir, M., I., Ashraf, N., Shahid, W., Afzal, D., Idrees, F., Ahmad, “Fundamentals of Density Functional Theory: Recent Developments, Challenges and Future Horizons.,” 2021, [Online]. Available: doi: http://dx.doi.org/10.5772/intechopen.99019 %0A%0A

[54] K. Burke, “Perspective on density functional theory,” no. Xc, pp. 1–10, 2012.

[55] M. A. Iqbal, N. Ashraf, and W. Shahid, “Fundamentals of Density Functional Theory : Recent Developments , Challenges and Future Horizons,” pp. 1–16.

[56] G. T. Hohenberg-Kohn, “theorem for nonlocal external potentials.,” *Phys. Rev.*, vol. 12, no. 6, p. 2111, 1975.

[57] and S. L. Kohn W, “Self-consistent equations including exchange and correlation effects,”

Phys. Rev., vol. 140, no. 4A, p. A1133, 1965.

[58] J. Chen, Z. Xu, and Y. Chen, "Introduction of density functional theory," *Electron. Struct. Surfaces Sulfide Miner.*, pp. 1–12, 2020, doi: 10.1016/b978-0-12-817974-1.00001-6.

[59] and C. C. Hamann, D. R., M. Schluter, "Norm-conserving pseudopotentials," *Phys. Rev. Lett.*, vol. 43, pp. 1494–1497., 1979.

[60] K. Kokko, P. T. Salo, R. Laihia, and K. Mansikka, "First-principles calculations for work function and surface energy of thin lithium films," *Surf. Sci.*, vol. 348, no. 1–2, pp. 168–174, 1996, doi: 10.1016/0039-6028(95)01029-7.

[61] D. Ji, Q. Zhu, and S. Wang, "Surface Science Detailed fi rst-principles studies on surface energy and work function of hexagonal metals," *Surf. Sci.*, vol. 651, pp. 137–146, 2016, doi: 10.1016/j.susc.2016.04.007.

[62] P. G. and J.-M. Albina, C. Els asser, J. Weissmuller and Y. Umeno, "Ab initio investigation of surface stress response to charging of transition and noble metals.," *Phys. Rev. B 85,* vol. B 85, no. 125118, 2012.

[63] J. W. uller and F. E. F. Weigend, "Structural relaxation in charged metal surfaces and cluster ions.," *Small*, vol. 2, pp. 1497–1503, 2006.

[64] J. K. S. and K. P. C. W. Haiss, R. J. Nichols, "Linearcorrelation between surface stress and surface charge in anion adsorption on Au(111).," *J. Electroanal. Chem.*, vol. 452, pp. 199–202, 1998.

[65] M. Shehu *et al.*, "First-principles insights into sulfur oxides (SO2 and SO3) adsorption and dissociation on layered iron sulfide (FeS) catalyst," *Mater. Today Commun.*, vol. 34, no. November 2022, p. 105452, 2023, doi: 10.1016/j.mtcomm.2023.105452.

[66] P. Pitriana, T. D. K. Wungu, H. Herman, and R. Hidayat, “The computation parameters optimizations for electronic structure calculation of LiPbl 3 perovskite by the density functional theory method,” *IOP Conf. Ser. Mater. Sci. Eng.*, vol. 434, no. 1, 2018, doi: 10.1088/1757-899X/434/1/012026.

[67] L. Vitos, J. Kolla, and R. Ahuja, “ (,” 2003, doi: 10.1103/PhysRevB.68.245417.